Check for updates

From molecular to supramolecular electronics

Hongliang Chen[1,2,3]✉ *and J. Fraser Stoddart*[1,2,3,4]✉

Abstract | Using individual molecules as conducting bridges for electrons offers opportunities when investigating quantum phenomena that are not readily accessible from experiments involving ensembles of molecules. The probing of single molecules has led, over the past few decades, to the rise of molecular electronics. Although single-supermolecule electronics is an emerging field, it is not yet a well-defined area of molecular electronics. There is little doubt, however, that single-supermolecule electronics is poised to have an impact on molecular electronics for the simple reason that non-covalent interactions between molecular components in complexes have a profound effect on electron conductivities. In this Review, we survey this emerging field from the standpoint of non-covalent interactions in mechanically interlocked molecules, as well as in supermolecules, and discuss the (super)structure–property relationship of four different interactions associated with (supra)molecular junctions. They are host–guest interactions, hydrogen bonding, π–π interactions, and non-covalent interactions present in mechanically interlocked molecules. We focus our attention on providing a supramolecular-level understanding of charge transport behaviour associated with each interaction, as well as demonstrating the theoretical background and experimental readiness of single-supermolecule electronics for potential applications, such as nucleic acid and peptide sequencing, and the design and production of quantum interference devices, random-access memories and integrated devices.

The way in which electrons propagate through a single molecule, which is the focus of molecular electronics[1], has been investigated now for almost half a century[2–5]. Multidisciplinary efforts — by physicists, chemists, biologists, material scientists and electronic engineers — have evolved within the discipline of single-molecule electronics[6–11] (SME), in which the ultimate goal is to use individual molecules as the active species in sustaining charge transport in electronic circuitry. Structure–property relationships between single molecules and their conductances have been investigated in considerable detail[12–19]; but to progress towards the fabrication of practical electronic devices, opportunities could well arise from the manipulation of weak, multiple interactions at a supramolecular level[20]. This burgeoning area of research, which we will call single-supermolecule electronics (SSE; BOX 1) is not yet a well-defined and appreciated addition to the field of molecular electronics. So far, single supermolecules have been investigated[21,22] in the same way as single molecules. On the contrary, SSE has the potential to expand the reach of SME because it not only focuses on charge transport within individual supermolecules, but also takes into account the weak non-covalent interactions between the components of supermolecules.

The focus of SSE (BOX 1) is on non-covalent interactions and on the properties of supermolecules as conducting species. In this context, supermolecules[20] — in which the interactions[23–26] within complexes can be radical in nature as well as ionic, and dynamic covalent or non-covalent (for example, hydrogen bonding) — represent a large family of molecules. Mechanically interlocked molecules[27] (MIMs), which, because of the presence therein of non-covalent interactions, exhibit[28] many of the features of supermolecules, are also promising candidates in the development of molecular electronics (FIG. 1). These interactions, which span almost all length scales, can profoundly affect the conductances of electronic devices, giving supermolecules and MIMs emergent properties not observable in their individual components. Careful investigations of SSE systems assist in bridging the gap between SME and single-molecule bioelectronics by manipulating non-covalent interactions at the single-(super)molecule level, harnessing molecular recognition properties of different components (MIMs) and complexes (supermolecules) for the efficient conversion of chemical information into electrical signals, and integrating single-molecule platforms with quantum tunnelling in the case of DNA, RNA and peptide sequencing.

[1]*Department of Chemistry, Northwestern University, Evanston, IL, USA.*

[2]*Stoddart Institute of Molecular Science, Department of Chemistry, Zhejiang University, Hangzhou, China.*

[3]*ZJU-Hangzhou Global Scientific and Technological Innovation Center, Hangzhou, China.*

[4]*School of Chemistry, University of New South Wales, Sydney, New South Wales, Australia.*

✉*e-mail: hongliang.chen@northwestern.edu; stoddart@northwestern.edu*

https://doi.org/10.1038/s41578-021-00302-2

Box 1 | **Defining single-supermolecule electronics**

Supramolecular chemistry was defined by Jean-Marie Lehn as "chemistry beyond the molecule", bearing on the organized entities of higher complexity that result from the association of two or more chemical species held together by non-covalent interactions. Its development requires the designed manipulation of non-covalent interactions so as to form supermolecules.

Supermolecules. Complexes of two or more molecules that are bonded non-covalently.

Mechanically interlocked molecules (MIMs). Molecules with entanglements in space between two or more component parts such that they cannot be separated without breaking or distorting chemical bonds between atoms. MIMs, because of the presence therein of non-covalent interactions, exhibit many of the features of supermolecules.

Component part. A group of atoms, or 'molecular entity', comprised of chemical bonds, which is mutually engaged in mechanical bonding with another molecular entity (as illustrated in the figure).

Single-supermolecule electronics (SSE). The investigation and application of non-covalently bonded superstructures for the construction of electronic devices.

The identification of MIMs as supermolecules is a common misnomer in the literature. Practically speaking, the boundaries between MIMs and supermolecules are always blurred — for example, in the case of pseudorotaxanes, which lack stoppers that are sufficiently bulky to prevent slippage of rings from dumbbells (see figure). The only distinction between rotaxanes and pseudorotaxanes is the height of the activation barrier and the corresponding kinetics that govern the timescale during which slipping of rings from dumbbells occurs.

In the language of supramolecular chemistry and mechanostereochemistry, we reiterate that MIMs are molecules, rather than supermolecules. In the field of molecular electronics, however, our focus is on non-covalent interactions and the properties of molecules as conducting species. The subtle differences between MIMs and supermolecules do not affect the intrinsic charge transport characteristics of conducting kernels. To aid in the discussion, we merge these two terms, MIMs and supermolecules, and discuss them under the umbrella of single-supermolecule electronics (SSE). There are two focuses in SSE: investigating the influence of non-covalent interactions on charge transport, and using single-molecule techniques to investigate the intrinsic characteristics of non-covalent interactions.

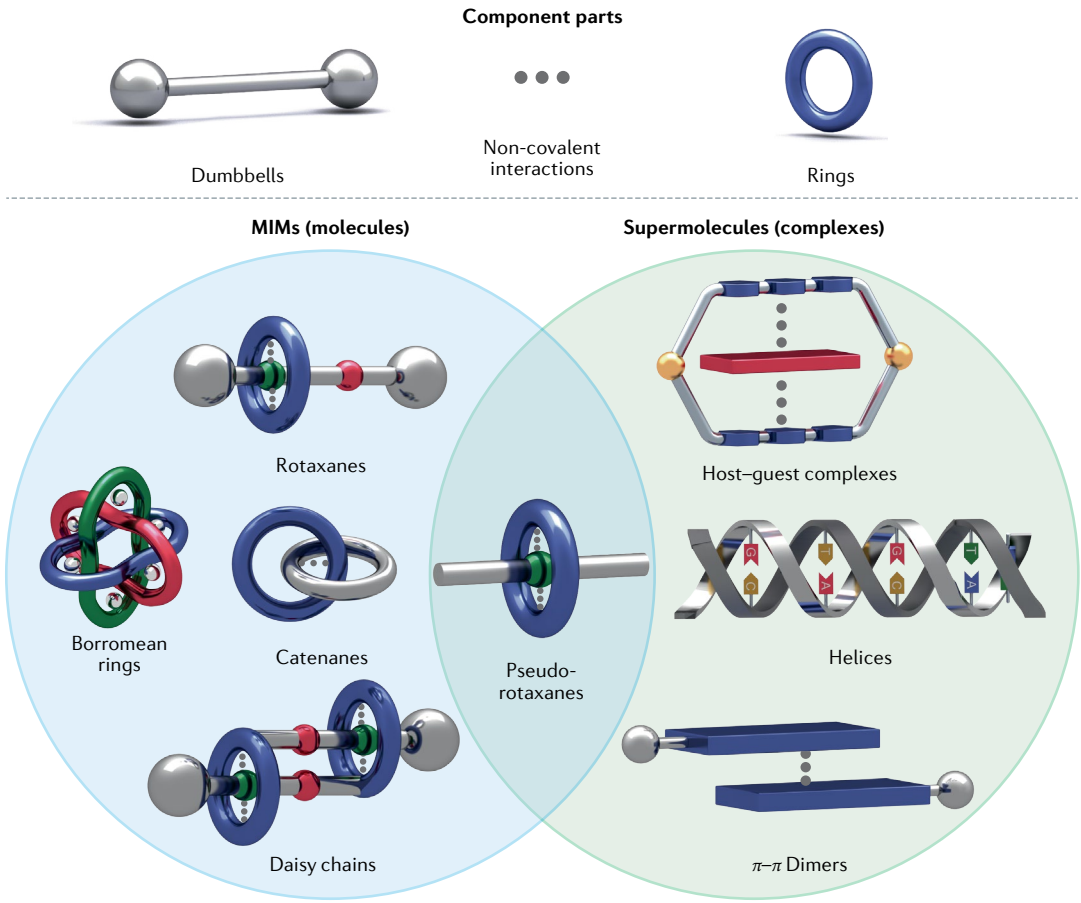

Reviews[9–11] on molecular electronics have more often than not been written from the viewpoint of those engineers and scientists who design molecules, fabricate electronic devices and measure conductances[8,15,17–19,29,30]. Consequently, the link between non-covalent interactions and charge transport has seldom, if ever, been the focus of such articles. Addressing this omission could do much to answer questions that arise from the increasing complexity associated with introducing multiple weak interactions into molecules (MIMs) and complexes (supermolecules). In this Review, we address three questions. The first question relates to how we can investigate

the details associated with non-covalent interactions at the single-molecule (MIMs) and single-supermolecule levels[22]. The second question relates to how we interpret the changes in charge transport brought about by the presence of non-covalent interactions and how we can use the interpretations to guide the design of switches, transistors and superconductors[31]. The third question relates to how we can make use of the chemist's expertise in handling (super)molecules and biomolecules to produce a fundamental understanding of biological processes such as DNA-mediated charge flow, protein folding and enzyme catalysis[32].

In this Review, we merge the languages of supramolecular chemistry and molecular electronics in order to discuss SSE in the context of non-covalent interactions, be they present in molecules (MIMs) or complexes (supermolecules). We also survey the powerful methods that are available to carry out the characterization and manipulation of conductances of these molecules and complexes. We provide a fundamental understanding of charge transport phenomena associated with each kind of non-covalent interaction, as well as examining the emerging areas in SSE research, such as the time evolution of the interaction dynamics, quantum interference effects and quantum tunnelling sequencing. Finally, we explore the potential opportunities for SSE and the technical challenges that must be met if we are to make progress towards real applications.

Technical development for SSE

The fundamental motivation behind SSE is to use single-molecule techniques to probe non-covalent interactions, both experimentally and theoretically. Recent experimental advances include the construction[21] of functional devices, the demonstration[33–35] of biomolecule sequencing applications, the illustration[36–38] of how quantum interference influences charge transport and the interpretation[22,39] of how non-covalent interactions behave dynamically at the single-supermolecule level. These experiments aim to provide fundamental understanding of charge transport phenomena associated with non-covalent interactions, as well as to illustrate the device-engineering efforts directed towards creating supramolecular integrated circuits. Many detailed descriptions and comparisons of single-molecule testbeds have been provided in other reviews[8,30,40]. Here we concentrate on the technical advances associated with emerging experimental platforms for SSE. We start with the development of the most widely used break-junction techniques, focusing on their attributes, as well as their shortcomings, relevant for unveiling the charge transport mechanisms associated with non-covalent interactions. We go on to advocate the need to integrate conductance measurements — based on break-junction techniques — with other probe methods to understand structure–property relationships in supramolecular systems. We conclude by discussing transistor-like platforms, particularly those based on graphene electrodes, because these systems are suitable for extracting dynamic data associated with non-covalent interactions at the single-supermolecule level.

Break-junction techniques. We have to recognize the distinctive properties of supermolecules and MIMs as interacting systems and their ability to act in a collective manner in electronic devices. In this context,

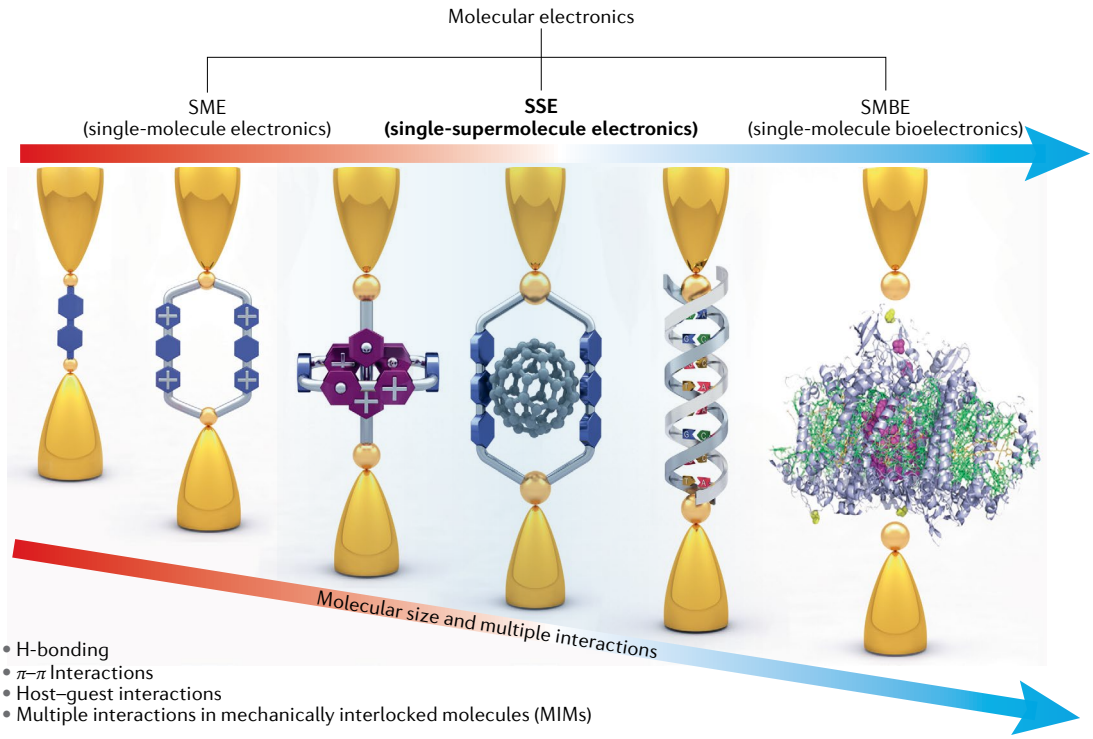

Fig. 1 | **Sub-fields within molecular electronics.** The figure shows the position of single-supermolecule electronics within the well-established field of molecular electronics.

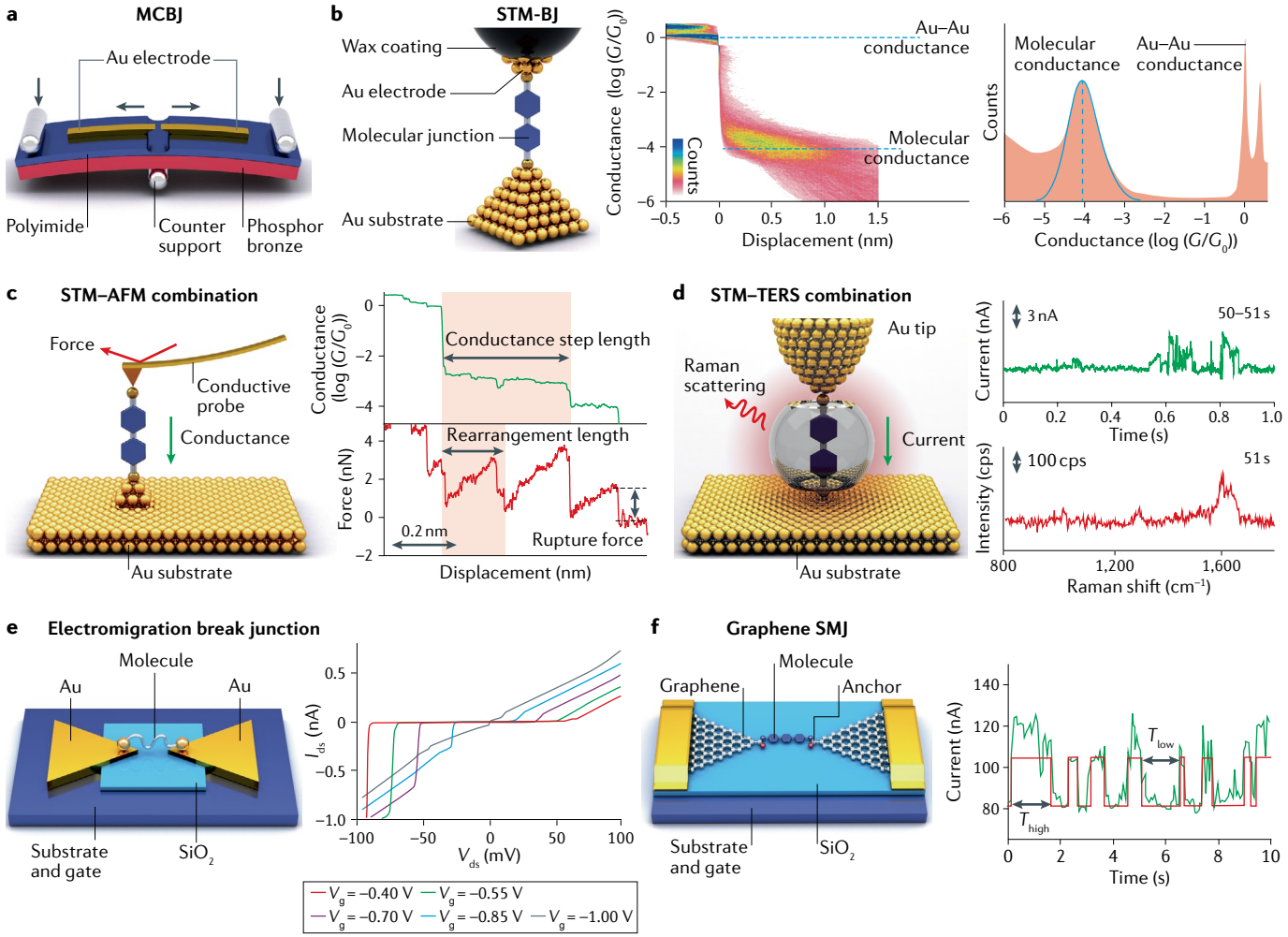

Fig. 2 | **Testbeds for single-supermolecule electronics. a** | Schematic illustration of a mechanically controlled break junction (MCBJ). **b** | Schematic illustration (left) of a scanning-tunnelling-microscope-based break junction (STM-BJ) and the corresponding 2D (middle) and 1D (right) histograms relating to molecular conductance, *G*. **c** | Schematic illustration of a conductive atomic force microscope (AFM) platform (left) for simultaneous single-molecule measurements (right) of current (green) and force (red). **d** | Schematic illustration (left) showing an STM-BJ integrated with tip-enhanced Raman spectroscopy (TERS) for simultaneous measurements (right) of the current (green) and corresponding TERS spectra (red) for a duration of 1 s. cps, counts per second. **e** | Schematic illustration of an electromigration break junction (left) and current-voltage curves (the voltage here refers to the bias voltage, V_{ds}) for different gate voltages, V_g (right). **f** | Schematic illustration of a graphene single-molecule junction (SMJ, left) and current-time curve (right, green) with the corresponding idealized fit (red), showing the fluctuation of current. T_{high} and T_{low} refer to the time intervals of the high and low-current states, respectively. Panel **c** is adapted from REF.[65], Springer Nature Limited. Panel **d** (right) is adapted from REF.[72], Springer Nature Limited. Panel **e** (right) is adapted from REF.[106], Springer Nature Limited. Panel **f** (right) is adapted from REF.[111], AAAS.

the break-junction technique — a powerful method for probing the charge transport in single-molecule electronics — also applies to single supermolecules. There are two mainstream break-junction platforms: mechanically controlled break junctions (MCBJs, FIG. 2a), and scanning-tunnelling-microscope-based break junctions (STM-BJs, FIG. 2b). These two methods, although differing in contact geometry, share working mechanisms and data processing methods. For example, in STM-BJ measurements, a metallic tip encroaches upon a metallic substrate to form a metal–metal contact. On retraction, the metal contact breaks, forming an atomically sharp tip that can pick up a (super)molecule, whether it is adsorbed on a substrate or dissolved in a solution, and finally creates a single-(super)molecule junction, which can be investigated during the course of elongation. Single-(super)molecule conductance is measured repeatedly as a function of this displacement, and hence is called a breaking trace. Thousands of breaking traces are used to plot 2D (FIG. 2b, middle) and 1D (FIG. 2b, right) histograms to illustrate the conducting signatures of (super)molecules.

When break-junction techniques are used in SSE, it is possible to gain some qualitative insights into charge transport behaviour associated with non-covalent interactions by designing control experiments involving mechanical switching[41] in host–guest complexes, charge transfer[42,43] on exposure to electronic dopants, and solvent-induced gating[44] by interacting with molecular wires. The conventional analysis of histograms,

however, disguises the rich physics associated with such weak interactions. In this situation, correlation analyses of breaking traces can be used[45,46] to provide more dynamic information during the formation and evolution of (supra)molecular junctions. In addition, gating in breaking junctions has been used to probe[47] charge transfer processes in host–guest complexes. With electrochemical gating in solution, supermolecules and MIMs can undergo[29,48] bistable co-constitutional changes, laying the foundations for building switches, transistors and memory devices.

Furthermore, 'soft' STM techniques[49,50], in which the tip is brought to a predetermined height before compression–elongation cycles, are promising options for manipulating and probing weak and dynamic non-covalent interactions. Particular attention has to be paid, however, when interpreting results. Additional complicating factors — namely, the effect of thermal fluctuation and changes in contact geometries — must be excluded before discussing the influence of non-covalent interactions. Lastly, by integrating such tunnelling techniques with nanopore platforms and machine-learning algorithms, much progress has been achieved[33–35,51–53] in sequencing biopolymers, paving the way for future commercialization.

Integrating conductance measurements with other techniques. Conductance measurements[30] on supermolecules and MIMs at (supra)molecular junctions performed simultaneously with the probing of some other properties — mechanical, optoelectronic, thermoelectric and spintronic properties — can be used to enhance our understanding of the structure–property relationships associated with non-covalent interactions, and provide different perspectives when interrogating these properties and the inherent correlations between them. Force spectroscopy, based on atomic force microscopy (AFM), has emerged as an attractive method for the control and probing of inter- and intramolecular forces in supermolecules[54], MIMs[55–58] and biomolecules[59,60]. By using a conducting AFM tip (FIG. 2c, left), force and conductance can be measured and correlated[61–65] simultaneously (FIG. 2c, right). So far, this platform has not been applied widely to either supermolecules or MIMs on account of technical incompatibilities associated with their structural complexity.

Supermolecules and MIMs are nearly always fairly large entities, a characteristic that leads to a decrease in conductivity. In force measurements, to shift the molecular signal away from the large additional peak related to gold rupture, long flexible linkers are nearly always inserted between the anchor and backbone, a manoeuvre that further reduces the conductivity of large entities. Although a stiff cantilever can be used to break the Au–Au metallic contact between the tip and the substrate, it is at the cost of low force resolution. To obtain a balance between force and conductance measurements, there are three directions worthy of exploration. One can use a molecular engineering strategy to make conductive supermolecules[48,66], or explore the possibility of resonant transport in MIMs through donor–acceptor or radical-pairing interactions. Another direction involves modulating the movement of a piezotransducer by using an ultra-sensitive feedback control system to isolate the Au–Au contacts in order to obtain a close relationship between force and conductance[67,68]. Finally, there is the possibility of introducing the q-Plus technique to single-molecule platforms[69,70]. q-Plus enables conductance measurements in STM mode and force measurements based on frequency shifts, both with high resolution.

Compared with the force–conductance combination, the integration of conductance with optical properties is well established[71]. Using light as a stimulus to activate a molecule and modulate the conductance is not the focus of this Review. Instead, the inherent single-molecule optical properties, associated with Raman[72–76], fluorescence[77,78] and electroluminescence[79,80] signals, are of fundamental interest if we wish to understand how non-covalent interactions behave when single supermolecules undergo geometrical changes. Tip-enhanced Raman spectroscopy[81] (TERS) promises to be a useful tool with which to carry out this work, because TERS provides a nanocavity between the tip and substrate, while retaining the tunnelling geometry. Host–guest chemistry[82–84] — for example, cucurbit[7]uril[85] accommodating one methylene-blue dye molecule as a guest inside its cavity — has been used to create a plasmonic nanocavity[86–88] (FIG. 2d, left) in order to isolate and protect guest molecules. With the superior control of junction stability at ultra-high vacuum and low temperatures, the STM–TERS platform enables chemical mapping[89,90] of a single molecule. When operated at room temperature and under ambient conditions, however, a mismatch with junction lifetimes appears during Raman and current measurements. In this situation, a fishing-mode STM–TERS[72] with a junction lifetime of several seconds can be introduced to obtain the conductance data and TERS spectra simultaneously from a molecular junction (FIG. 2d, right).

Finally, we highlight the fact that the MCBJ platform, with its horizontal contact geometry, is more compatible than STM-BJ platforms with conventional optical microscopes used in surface-enhanced Raman scattering[73,91] (SERS) and microelectromechanical system (MEMS)-based chip fabrication[76]. However, technical challenges similar to those encountered with STM–TERS exist in the case of MCBJ–SERS. Despite these technical challenges, the ability of supramolecular chemists to encapsulate guest molecules inside host nanocavities eases the burden of positioning the electrodes on the nanoscale. In the future, by using laser cooling[92–94] and optical trapping[95–99] techniques, which have already been used to trap small molecules[100], nanomaterials[101] and biomolecules[102–104], we will come much closer to the ultimate goal of manipulating[105] and probing the dynamics of non-covalent interactions and even chemical reactions involving single molecules.

Solid-state platform with transistor-like configurations. Break-junction techniques, together with their combination platforms, are particularly suitable for high-throughput testing of a series of molecules with similar structures. These methods face the problem

of short junction lifetimes and the challenge of scalability. By contrast, transistor-like solid-state platforms meet the needs perfectly for durability, scalability and stability. First, these devices are fabricated directly on the gate dielectrics (FIG. 2e, left), enabling strong gate control[106,107] of current–voltage characteristics (FIG. 2e, right) and low-temperature probing of intrinsic transport properties. Stronger gate coupling can be achieved by replacing SiO_2 dielectrics with high dielectric constant materials[108] or ionic liquids[109]. Second, graphene and carbon nanotubes can serve as alternative electrode materials that form more stable point contacts with (super)molecules (FIG. 2f, left), either covalently[22,110,111] or non-covalently[112–115]. Two methods — feedback-controlled electroburning[112] and electron-beam lithography[116] (EBL) — have been used to introduce nanogaps with high precision, with EBL showing the better performance in device upscaling and circuit patterning. Lastly, owing to their superior stabilities, graphene-based junctions, engineered with local chemical gates[39,111], enable the investigation of the dynamics of non-covalent interactions at the single-supermolecule level (FIG. 2f, right).

Technical challenges also exist in these transistor-like platforms. First, the junction formation yields are far too low to meet the needs of mass production and device integration. Their electrical conductance uniformity shows some dependence on factors such as the processing history, anchoring strategies and contact geometries. Second, at a fundamental level, each molecular junction requires a new device to be fabricated, a process that is time-consuming when studying a series of (super)molecules with similar (super)structures. Third, special attention has to be paid when interpreting data acquired from electroburning graphene-based junctions because of the formation of graphene quantum dots or the attachment of contaminants during processing. The recent introduction of new geometries into graphene-based devices has led to an increase in electronic and mechanical stability[117–120]. It is likely that the ultimate solution to all these challenges will lie in the precise etching[121] of graphene electrodes — that is, accurate control over the gap size between pairs of graphene electrodes, and the realization of atomically smooth and configuration-specific graphene electrode edges. With a suitable choice of molecules or supermolecules, this technique holds considerable promise for their use as electronic elements and their future integration into functioning chips.

Molecular circuits based on macrocycles

The elegance of quantum ring structures, with sizes ranging from the nanoscopic to the mesoscopic scale, attracts considerable attention[122] because of a series of quantum effects correlated to the phase of the electron wavefunction. Further investigations on such ring-like structures have revealed additional quantum phenomena, including the onset of persistent currents[123], Kondo effects[124], electron–electron interactions[125] and the possibility of spintronic applications[126,127]. Theoretical and experimental studies have demonstrated that scattering affects phase-coherent transport on the mesoscopic scale. The search for smaller scatter-free structures drives exploration in the field of synthetic quantum rings[128–130] — namely, conjugated macrocycles. When fully conjugated aromatic macrocycles are placed in a magnetic field, the ring current can be predicted[131,132] by Hückel's rule and regulated[132–135] by changing the macrocycles' topologies, constitutions, conformations and oxidation states. To probe ring currents at the single-molecule level, anchor groups need to be installed on the ring, creating another research field, that of topology-driven molecular circuits[136,137]. In this case, it is helpful to consider a macrocycle as equivalent to a macroscopic circuit in which quantum interference[36–38,138] may take place between two conducting channels. Furthermore, these macrocycles have the ability to host one or more guest molecules, causing great changes in their molecular conductances[41,47]. In this section, we summarize the trends of using macrocycles to construct intramolecular circuits, as well as their electrical responses when they host guest molecules.

Towards the construction of intramolecular circuits. Macrocycles, which have multiple conducting channels, are often used to construct intramolecular circuits[2] to aid the development of emerging technologies, such as molecular calculators[139], single-molecule transistors[140,141] and quantum logic gates[142,143]. In these electronic architectures, charge transport is dominated mainly by quantum effects, and most importantly, the electronic communication between different conducting channels becomes non-negligible under certain circumstances. In this subsection, we summarize three quantum effects — quantum interference effects, gating effects and the combination of both — to manipulate the conductivity of macrocyclic circuits.

First, when electrons propagate through two identical parallel channels in a macrocyclic circuit (FIG. 3a, top), quantum interference dominates the charge transport. In general, quantum interference is used to predict electron transport behaviour through delocalized backbones, indicating that the charge transport at molecular junctions is determined by the phase and amplitude of the highest occupied and lowest unoccupied molecular orbitals (HOMO and LUMO). The orbital selection rule[13,144,145], originating from Green's functions in zeroth order, is used to rationalize the occurrence of quantum interference. The quantum interference mechanism, however, can also be interpreted[138,146,147] as the superposition of local contributions of each transport path through a molecule by considering the orbital interactions between them. In this regard, by comparing[36,37] the conductance of a two-channel macrocycle with its one-channel control, we can obtain the total increase in conductance, which is larger than the classical value of 2 obtained from Kirchhoff's circuit law. Such an increase in conductance (FIG. 3a, bottom) can be ascribed to a cross term arising from constructive quantum interference.

Second, the charge transport in macrocyclic circuits can be controlled by an external potential (FIG. 3b, top) — namely, electrochemical gating — that shifts the transmission spectrum near the Fermi level (FIG. 3b, bottom).

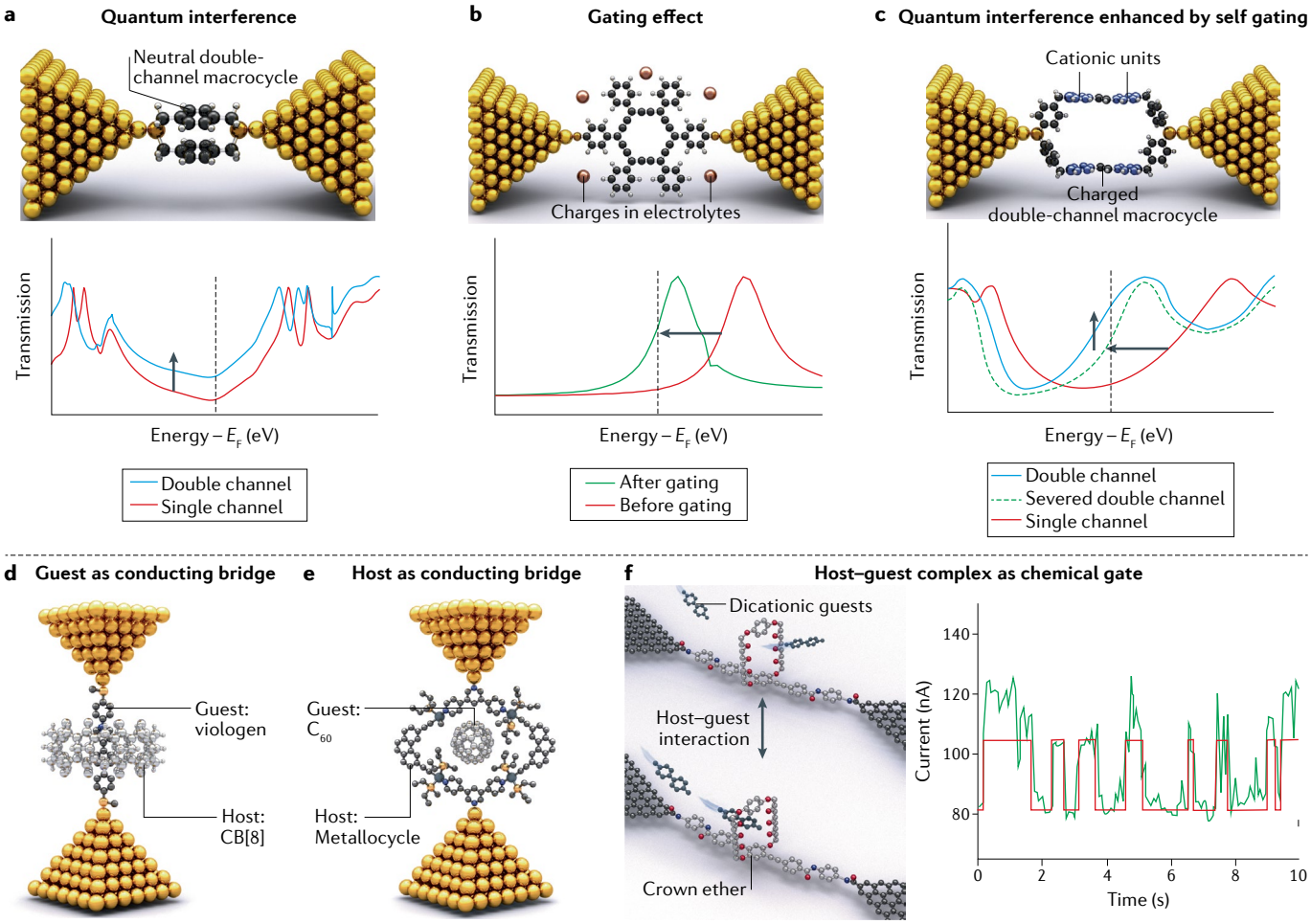

Fig. 3 | **Molecular circuits based on macrocycles and host-guest complexes. a** | Schematic illustration (top) and transmission spectra (bottom) of an intramolecular circuit across a neutral double-channel macrocycle in which quantum interference dominates the transport. **b** | Schematic illustration (top) and transmission spectra (bottom) of an electrochemically gated intramolecular circuit in which the conductance is controlled by gating effects. **c** | Schematic illustration (top) and transmission spectra (bottom) of an intramolecular circuit across a double-channel charged macrocycle whose conductance is determined by interchannel gating and quantum interference. **d** | Schematic illustration of a viologen ⊂ CB[8] complex in which the viologen guest conducts the current. **e** | Schematic illustration of a C_{60} ⊂ metallocycle complex in which the macrocyclic host conducts the current. **f** | Left, schematic illustration showing the dynamic host-guest interactions when a dicationic viologen threads through a crown ether. Right, current-time curve showing current fluctuations (green) with an idealized fit (red). The high and low current levels are attributed to the complex formation and deformation states, respectively. CB[8], cucurbit[8]uril; E_F, Fermi energy. Panel **a** is adapted from REF.[37], Springer Nature Limited. Panel **b** is adapted from REF.[148], Springer Nature Limited. Panel **c** is adapted with permission from REF.[38], Elsevier. Panel **d** is adapted from REF.[47], CC BY 4.0 (https://creativecommons.org/licenses/by/4.0/). Panel **e** is adapted from REF.[41], CC BY 4.0 (https://creativecommons.org/licenses/by/4.0/). Panel **f** is adapted with permission from REF.[111], AAAS.

For example, the molecular conductance of a graphyne-like macrocycle, owing to its rigid and planar conformation, shows a 40-fold increase[148] compared with the flexible single-channel control provided by only one loop of the macrocycle. Quantum interference is not dominant in this graphyne-like macrocycle, perhaps owing to the occurrence of a near-resonant transport[115] close to the Fermi level. The small HOMO–LUMO gap, however, can be electrochemically gated, achieving an order of magnitude increase in junction conductance. Quantum interference in conjugated molecules can be manipulated[149–151] effectively through electrostatic gating by tuning the molecule in and out of anti-resonance. By using holistic molecular design, such a control strategy can be implemented in macrocyclic circuits to realize multimode control over conductances.

Third, and specifically related to macrocycles with strong interchannel interactions[38] (FIG. 3c, top) — for example Coulombic interactions occurring between charged parallel channels — the interchannel gating effect and quantum interference can coexist. The effective conductance of each channel is promoted by the interchannel gating effect, causing the transmission curve to shift leftwards (FIG. 3c, bottom) to achieve near-resonant charge transport. Furthermore, the total conductance of a macrocyclic circuit is enhanced by constructive quantum interference, triggering an upward shift of the transmission curve (FIG. 3c, bottom),

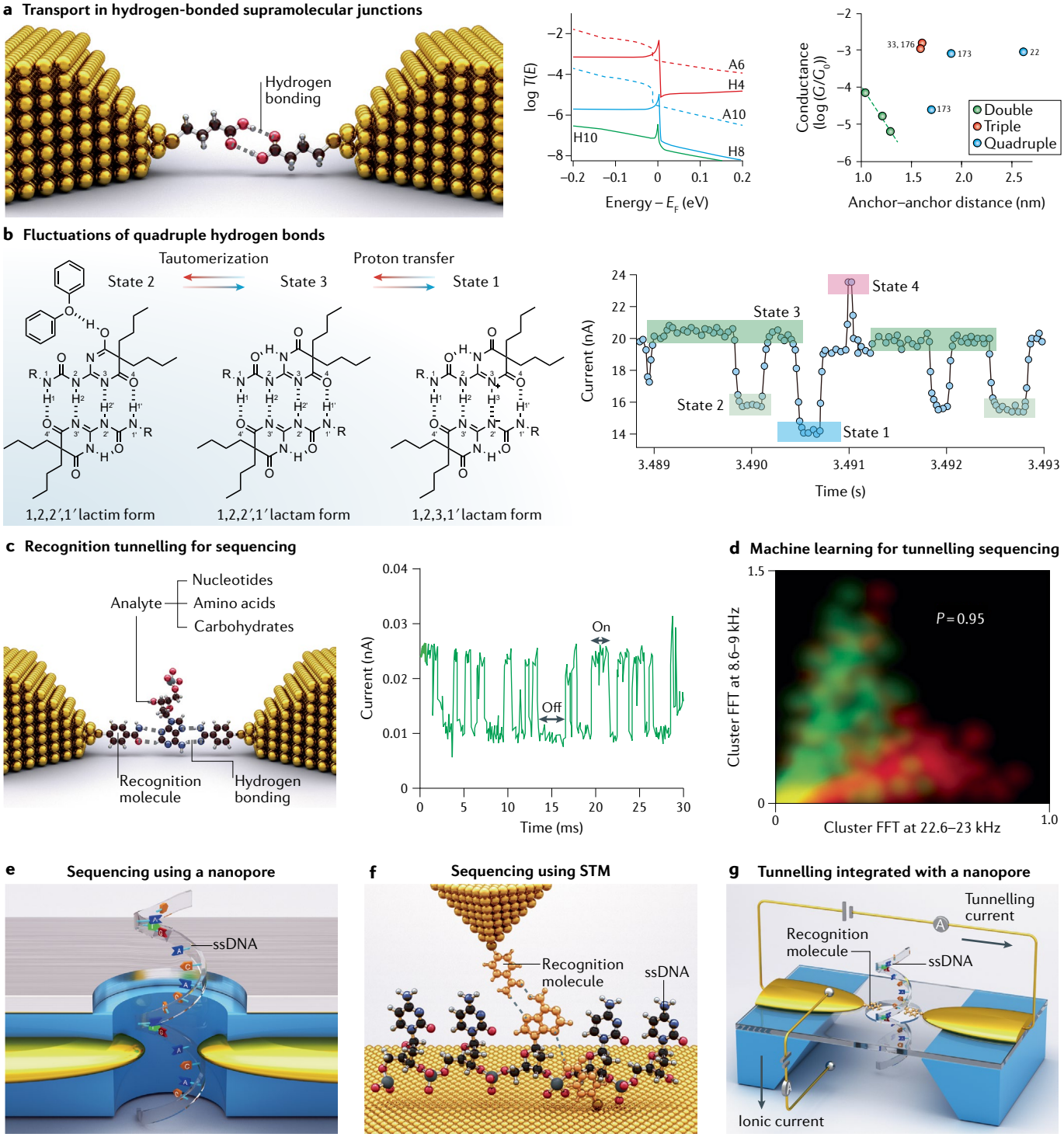

and finally leads to a 50-fold conductance increase. In future work, through the controllable perturbation of interchannel interactions or quantum interferences, it should be possible to achieve dual-mode control[152] over molecular conductances.

Host–guest interactions at the single-supermolecule level. Macrocycles provide a molecular platform whence to gain an understanding of the effects of interchannel interactions on charge transport. Moreover, they can also be used as host molecules, following the formation of complexes with guest molecules, in order to clarify the influence of host–guest interactions on charge transport. There are three experimental scenarios in the case of supramolecular systems, differing in the role that host and guest molecules play in conducting electricity, that can be used to probe host–guest interactions.

In the first scenario, the guest molecule behaves as the conducting bridge that allows us to study the influence of the macrocyclic host. For example, the molecular conductance of viologen bridges increases[47] upon complexation (FIG. 3d) with cucurbit[8]uril. The conductance

◀ Fig. 4 | **Hydrogen-bonding investigation focusing on applications in tunnelling sequencing. a** | Transport in hydrogen-bonded supramolecular junctions. Left, schematic illustration showing a hydrogen-bonded supramolecular junction. Middle, transmission ($T(E)$) spectra showing the Fano resonance induced by hydrogen bonding near the Fermi level, E_F. A6 and A10 refer to two alkanedithiols with a length of six and ten carbons, respectively. H4 and H8 refer to two carboxylated alkanedithiol dimers with a length of four and eight carbons, respectively. Right, conductance of multiple hydrogen bonding with respect to molecular length. Results are from REFS[22,33,173,176]. **b** | Fluctuations of quadruple hydrogen bonds. Left, schematic diagram showing the reversible reactions involved in quadrupole hydrogen-bonding dynamics. Right, current-time curve showing distinct current levels that correlate with four states in hydrogen-bonding dynamics. **c** | Recognition tunnelling for sequencing. Left, schematic illustration showing the recognition tunnelling set-up with recognition molecules adsorbed on a pair of closely spaced electrodes. The analytes (nucleotides, amino acids or carbohydrates) are captured by the recognition molecules through hydrogen-bonding interactions. Right, current–time curve showing the tunnelling currents conducted via single-base molecules. **d** | Machine learning for tunnelling sequencing. 2D plot of probability density as a function of the two fast Fourier transform (FFT) feature values. The colours red and green refer to the data points for amino acids mGly and Leu, respectively. The yellow region indicates overlapping data. The final analysis accuracy P is 95%. **e** | Schematic illustration showing a single-strand DNA (ssDNA) molecule translocating through a nanopore embedded with tunnelling electrodes. **f** | Schematic illustration showing the recognition tunnelling sequencing of DNA with a scanning tunnelling microscope (STM). Both the gold tip and substrate are functionalized with recognition molecules. **g** | Schematic illustration showing a proposed multimode sequencing platform. Panel **b** is adapted from REF.[22], CC BY 4.0 (https://creativecommons.org/licenses/by/4.0/). Panel **c** right and panel **f** are adapted from REF.[185], Springer Nature Limited. Panel **d** is reprinted from REF.[34], Springer Nature Limited. Panel **e** is adapted from REF.[189], Springer Nature Limited.

increase originates from the reduced reorganization energy when establishing a complex. Host–guest interactions were also demonstrated to minimize the electrostatic repulsions between cationic conducting bridges in solution[153], thus stabilizing the charged supramolecular junctions at high concentrations.

In the second scenario, the macrocycle acts as the backbone that enables the detection of the conductance switching before and after accommodating a guest molecule (FIG. 3e). In this situation, the supramolecular design — including the conductivity and the cavity size of the host, the choice of the guest, the constitution of the anchor, and the binding affinity between the host and guest — should be considered as a holistic design. Any structural changes in the macrocycles will lead to considerable variations in conductance. As an example, the conductance of a metallocycle serving as a host — with a tailored cavity size — is increased[41] by approximately an order of magnitude after accommodating C_{60}. In addition, the conductance can be switched back to the initial level on release of the guest molecule upon mechanically stretching of the metallocycle. Given the structural complexity of macrocycles, the influence of many other factors on conductance, such as guest-mediated through-space transport, gating effects and quantum interference, should be considered in future research.

The third scenario is achieved[39,111] by covalently attaching the macrocycle to a conjugated molecular bridge so that it serves as an additional local gate (FIG. 3f, left). When a charged guest interacts with the host — for example, when a dicationic viologen threads through a crown ether — the charges can gate the channel electrostatically, modulate the carrier density therein, and induce irregular current spikes during real-time current measurements (FIG. 3f, right). This technique enables the direct monitoring of host–guest interactions at the single-supermolecule level, such as pseudorotaxane formation/deformation[111] and shuttling[39] processes. Furthermore, by analysing the current distribution between two current levels, the binding constants and activation energies can be quantified[111], a process that is generally carried out[154] from ensemble experiments in solution at equilibrium.

By investigating host–guest interactions at the single-supermolecule level, we can gain insight into the influence of host–guest interactions on charge transport, thereby achieving precise control over the conductance. Understanding how host–guest complexes behave at the single-supermolecule level also makes it possible to revisit fundamental aspects of supramolecular chemistry and introduce new techniques and practices into emerging areas, such as supramolecular polymerization[155], catalysis[156] and drug discovery[157].

Hydrogen bonding in tunnelling sequencing

Hydrogen bonding is ubiquitous in both biological and chemical systems and represents a powerful mechanism for constructing superstructures with desired building blocks through molecular recognition and self-assembly. Most importantly, the electron transport properties of intermolecular hydrogen bonds are critical in establishing[158] long-range electronic coupling in biomolecules such as proteins or cytochromes. In this section, we provide an understanding of hydrogen bonding at the single-supermolecule level, followed by an overview of how to identify single base pairs or amino acids through recognition tunnelling, and finally explore the applications of hydrogen-bonded supermolecules in nucleic acid and peptide sequencing.

Understanding hydrogen bonding at the single-supermolecule level. Evaluating how chemical bond strengths influence charge transport efficiency through a molecule has been a subject of interest for years[159]. Experimentally, many techniques have revealed that the efficiency of charge transport modulated by numerous weak hydrogen bonds acting cooperatively is comparable with[160–164] or even higher than[165,166] that of the charge transport involving stronger σ-bonds. We examine the role of hydrogen bonding in single-supermolecule charge transport, because single-molecule techniques could offer new insights into long-standing questions such as the root cause of the conductance difference between hydrogen bonds and σ-bonds, the origins of the large conductance variations between double, triple and quadruple hydrogen bonds, and the dynamics of hydrogen-bond formation.

The effect of bond strength on transport properties is generally evaluated by comparing the conductance of hydrogen-bonded and covalently bonded model systems with similar (co)-constitutions. Experimental investigations[167] reveal that, although hydrogen bonds (FIG. 4a, left) conduct electrons better than alkanes, for example, over short ranges, their conductance decays rapidly as the transport path becomes longer than 13 Å, showing a crossover in length-dependent conductance plots. Many theoretical investigations[168–170]

have been devoted to understanding mechanisms of hydrogen-bond-mediated charge transport, on account of its importance in both chemical and biological systems. Early theoretical investigations attributed[167] the enhanced conductivity of hydrogen-bonded supermolecules to the greater density of states of the hydrogen-bonding kernel. To explain both the crossover and exponential decay, a traditional viewpoint was invoked, considering the coupling efficiency between the hydrogen-bonded centre and the anchors attaching the supermolecules to the electrodes[171], as well as a new perspective (FIG. 4a, middle) that examined[172] the role of Fano resonance in the transmission curves near the Fermi energy.

A large number of experiments, in combination with theoretical investigations, can more or less depict the big picture of the conductance behaviour involving double hydrogen bonds. The situation, however, becomes much more complicated when dealing with the cooperative effects associated with multiple hydrogen bonds[173], hydrogen-bonded arrays[174] and hydrogen-bond-connected nanostructures[175]. Based on the experiments carried out so far, the measured[22,33,173,176] conductances (FIG. 4a, right) across supramolecular junctions with three or four pairs of hydrogen bonds span nearly two orders of magnitude, from $10^{-5}\,G_0$ to $10^{-3}\,G_0$, suggesting that the insertion of multiple hydrogen bonds into a supramolecular bridge changes the length dependence of charge transport. Besides, conductance shows a strong dependence[173] on the device test platforms, the anchors and the (co)-constitutions and (co)-conformations of the (super)structures, making both theoretical and experimental investigations challenging. The relatively high conductance associated with multiple hydrogen bonds[22,173], however, may encourage further exploration[177,178] towards understanding the electron transport mechanism from different angles, such as through the measurements of conductance integrated with force, which can be used to probe directly the correlation between hydrogen-bond strength and supramolecular conductances. Considerable future opportunities exist in the construction and testing of 1D hydrogen-bonded chains[174] and nanobelts[175], which are expected to show atypical electronic properties.

The binding energies associated with hydrogen bonds, which lie somewhere between 1 and 50 kJ mol^{-1}, are much lower than those of covalent bonds, leading to increased flexibility in hydrogen-bonded superstructures. At the microscopic level, the flexibility arises from three different processes[179]: the vibrational motion dynamics of the hydrogen bonds, the hydrogen atom or proton transfer reactions, and the forming and breaking of hydrogen bonds. These processes span a multitude of timescales, in which elementary events can occur within an ultrafast period of time, ranging from femtoseconds to picoseconds. Experimentally, the vibrational dynamics of hydrogen bonds can be investigated[179] by ultrafast vibrational spectroscopy in solution. Hydrogen/proton transfer reactions have been imaged[180–183] by STM under ultra-high-vacuum and low-temperature conditions. Real-time probing of hydrogen forming and breaking processes under normal conditions can be realized[22] with a solid-state device platform, for example by connecting a quadruple hydrogen-bonding kernel covalently to graphene electrode pairs to establish a stable supramolecular junction. Superstructural fluctuations of hydrogen bonds (FIG. 4b, left) — stochastic bond rearrangements through intermolecular proton transfers or lactam–lactim tautomerizations — can be correlated with the multilevel current signals, which can be classified into several states according to their amplitudes (FIG. 4b, right). All the approaches to probing the hydrogen-bonding dynamics are essential for understanding and manipulating charge transport with atomic precision, demonstrating the potential to build supramolecular switches.

Molecular recognition using hydrogen bonding. Tunnelling currents have been used by researchers for next-generation, direct sequencing of biomolecules[52,184]. The critical challenge that has confronted this field for a long time is how to achieve single-molecule detection and single-base discrimination. By using a hydrogen-bonding recognition strategy, researchers[33,34,53,185] are getting closer to achieving this goal. The method — named recognition tunnelling (FIG. 4c, left) — reads tunnelling currents flowing through target molecules between the nanogap electrodes modified with the recognition molecules. This method[35] allows the identification of individual canonical and modified chemical building blocks (for example, the sequences of nucleotides[33,185], amino acids[34] and monosaccharides[53]) in nucleic acids, peptides and carbohydrates. A series of carboxamide heterocycles have been used[185–187] to form hydrogen bonds with the analytes. Conjugated pyrene backbones have also been suggested as suitable candidates to explore[188] the possibility of π–π interactions as the recognition motifs. The accuracy of the readout can be improved by optimizing the design of recognition motifs through reducing or increasing hydrogen-bonding sites, or through extending conjugated aromatic π-systems.

When a DNA chain passes through a tunnel junction, different nucleobases will induce[185] fluctuations in the tunnelling currents (FIG. 4c, right). Further data processing is mainly based on histogram analysis[185,189] of current–time measurements. Histogram analysis, however, inevitably causes signal overlap of different base pairs in DNAs and different amino acids in peptides, leading to errors in discrimination. A machine-learning method (FIG. 4d) has been used[34] to overcome this dilemma. The algorithm is used as a classifier to deal with the fast Fourier transform (FFT) results of spike-like current–time signals and enables high-accuracy identification of DNA[188] and RNA[35] nucleotides, amino acids[34] and monosaccharides[53].

Recognition tunnelling testing platforms, in combination with machine-learning data processing, enable the quantitative evaluation and accurate discrimination of (super)structures that cannot be achieved by conventional methods, opening the way for real sequencing applications. Under a more ambitious blueprint[190], machine learning — together with density functional theory, molecular dynamics simulations and non-equilibrium Green's functions — can be used to

drive the design of recognition molecules, followed by high-throughput experimental screening to identify the ideal candidates. After several iterations, the best molecular design and the highest sequencing accuracy can be achieved. In this research, experiments and simulations can be mutually assiested and ultimately lead to fast and low-cost single-molecule sequencing.

Applications of nucleic acid and peptide sequencing. Tremendous progress has been made over the past decade, but considerable challenges remain when it comes to developing quantum tunnelling techniques for practical single-molecule sequencing of DNA, RNA and peptides[184] . These challenges are: controlling the random motion of the analytes; realizing single-molecule detection; achieving single-base resolution; and implementing error correction by integrating multiple sequencing techniques. In the initial step towards the construction of single-molecule quantum sequencing devices, solid-state nanopore platforms, integrated with nanogap electrodes, were fabricated[191,192] by electron-beam lithography (FIG. 4e). These devices, however, can only detect double-stranded DNA (dsDNA) translocation events, and fail to accomplish single-molecule resolution because of small tunnelling-current modulation. In the pursuit of single-molecule and single-base identification, an essential step is the fabrication[189] of nanogap electrodes whose gap size is comparable to the diameter of single-stranded DNA (ssDNA). In this research, STM-BJ and MCBJ-based platforms have been used[33,34,185] to identify single bases in solution (FIG. 4f). Furthermore, different bases can be discriminated by the hydrogen-bonding recognition tunnelling technique. Specific hydrogen-bonding interactions with recognition molecules improve the readout accuracy.

In a further step towards real sequencing applications, a proposed multiparameter DNA sequencing platform (FIG. 4g), integrating plasmonics[193], nanopores[51], embedded nanoelectrodes[191], recognition tunnelling techniques[33] and even SERS[194], allows the simultaneous measurements of ionic and tunnelling currents, and fluorescent and Raman signals. Integration improves the accuracy of current readout by multiparameter comparisons and error corrections, increasing the sensitivity and thus paving the way for real low-cost and solid-state next-generation sequencing devices.

Charge transport in π-stacked kernels

Measuring the charge transport through a single aromatic molecule, in which the π-electrons are delocalized throughout the plane of the molecule by through-bond π-conjugation[9], constitutes by far the best known experimental approach to the probing of aromatic molecules in SME. There exists, however, another (supra)molecular family, in which the π-electrons distribute themselves in the interplanar regions between the adjacent π-stacked aromatic molecules/units, giving rise to through-space π-conjugation. The essential distinction behind these two classes of aromatic molecules/units amounts to a difference in their relative geometrical disposition, leading to either through-bond or through-space transport mechanisms.

Through-space conjugation[195] is established as the result of multiple interactions — including short-range π–π or charge transfer interactions, and long-range dipole–dipole or Coulombic interactions — when aromatic molecules/units are aligned in a face-to-face manner so as to ensure overlapping of electron density distributions. Through-space transport is far from having been fully explored because of the lack of access to appropriate (supra)molecular systems. dsDNA represents a large family of naturally occurring π-stacked supermolecules, in which the aromatic base pairs are separated from each other by π–π stacking distances of ~3.4 Å. Such a superstructural geometry is commensurate with the overlap of electron density between adjacent base pairs, leading to efficient stacking and electronic conduction[196]. Superstructural similarities also exist between aromatic molecules/units in organic semiconductors[197–199] and in multilayer graphenes[200], where π–π stacking distances are also ~3.4 Å. At the single-supermolecule level, these π-stacked systems allow us to probe quantitatively the correlation between π–π coupling and charge transport. Here, we provide a supramolecular-level understanding of through-space conjugation and illustrate the control of charge transport in π-stacked (super)molecules, as well as discussing DNA-based nanoelectronics.

Fundamental understanding of through-space charge transport. During the past decade, many π-stacked kernels have been examined as conducting bridges, including, but not limited to, π-stacked benzene rings[201–203], π-stacked self-assembled cages[204–206], π-stacked dimers[207–210], π-foldamers[211,212] and bilayer graphenes[213–215]. Single-supermolecule investigations have disclosed that through-space π-conjugation can support the conduction of electricity as effectively as conventional through-bond π-conjugation. A better understanding of the through-space conduction would be beneficial to the engineering[216] of charge transport in organic electronics, optoelectronics and photovoltaics, in addition to the understanding[217] of the charge transport related to some biological processes in DNA, including DNA methylation[218] and intercalation[31,219,220], as well as electronic signal delivery[221].

Because direct probing[222] of supramolecular π-stacked systems is challenging, a compromise approach is to imitate π–π stacking intramolecularly. A strained [2.2] paracyclophane scaffold, which has been used[201] as a model system, has revealed a non-resonant mechanism of electron tunnelling through its π-stacked kernels. The conductance can be regulated by manipulating the stacking geometry by exerting a mechanical shear force on the [2.2]paracyclophane (FIG. 5a), which leads to pronounced conductance oscillations on account of quantum interference of frontier orbitals of the molecule. Another protocol, leading to through-space π-conjugation, is the use of a folding strategy (FIG. 5b and c), an approach that recalls[223] the influence of the secondary structure in proteins on charge transport. In this context, through-bond and through-space conjugation can be integrated[224,225] into one folded molecule (FIG. 5b), allowing for multiple conducting channels in a single-molecule device.

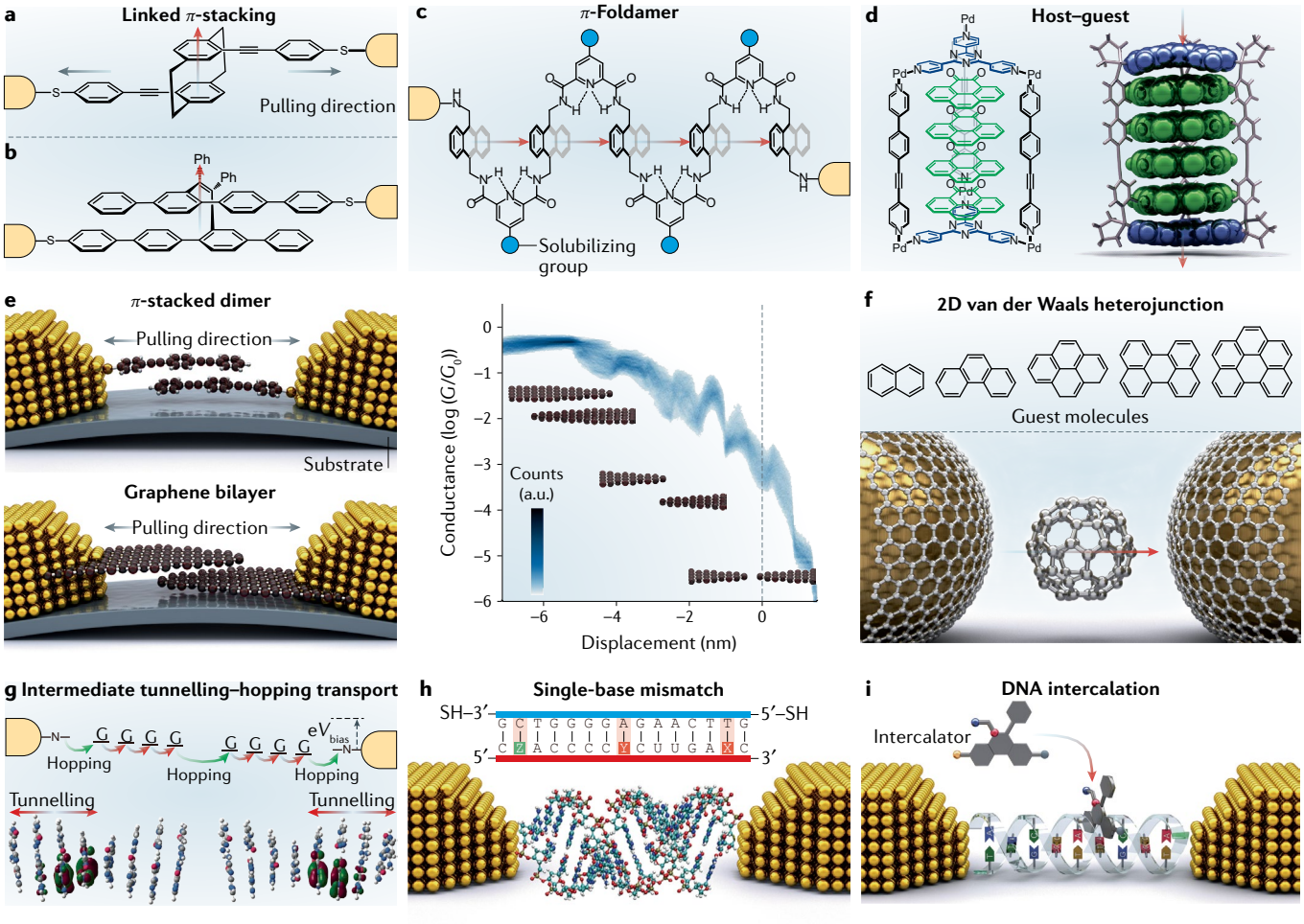

Fig. 5 | **Charge transport in π-stacked systems. a**-**c** | Simplified representations of intramolecular π–π stacking co-conformations. Panel **a** represents a strained [2.2]paracyclophane scaffold; panel **b** a folded molecule with multiple conducting channels; and panel **c** a π-foldamer. **d** | Superstructural formula and solid-state superstructure showing four π-conjugated guests stacked inside a cage host. **e** | Schematic illustration of a π-stacked dimer on a mechanically controlled break junction platform (top left), schematic representation of a stacked bilayer graphene junction (bottom left), and 2D histogram of breaking traces (right) showing oscillations on account of quantum interference effects. **f** | Schematic illustration showing the cross-plane break-junction set-up (bottom) and examples of possible 2D guest molecules (top): naphthalene, phenanthrene, pyrene, perylene and benzoperylene. **g** | Coherent and incoherent transport coexist in stacked DNA sequences. **h** | Schematic illustration showing the detection and identification of RNA point mismatch. **i** | Schematic illustration showing the insertion of an intercalator in DNA, which influences the DNA's charge transport. Panel **a** reprinted with permission from REF.[203], ACS. Panel **c** is adapted from REF.[211], CC BY 4.0 (https://creativecommons.org/licenses/by/4.0/). Panel **d** is adapted with permission from REF.[204], Wiley. Panel **e** bottom left and right are adapted from REF.[213], Springer Nature Limited. Panel **f** is reprinted from REF.[231], CC BY 4.0 (https://creativecommons.org/licenses/by/4.0/). Panel **g** reprinted from REF.[32], Springer Nature Limited. Panel **h** is adapted from REF.[251], Springer Nature Limited.

Another foldamer[211] — exhibiting the folded conformation through intramolecular π–π interactions (FIG. 5c) — affords an efficient through-space tunnelling channel across the π-stacked aromatic units.

These through-space conjugated molecules serve as model systems to elucidate the charge transport in π-stacked supermolecules. The conductance measurements, carried out so far on intramolecularly π-stacked molecules, support the big picture of coherent tunnelling[201,211], although some detailed transport mechanisms still need to be established. These molecules, however, are far from enabling the manipulation of molecular conductances needed for practical applications in molecular devices.

Controllable charge transport in π-stacked supermolecules. Electrons can propagate efficiently through π-stacked systems over long distances while maintaining a close association with the conjugation in the aromatic molecules themselves, the stacking distances between them, and the relative geometrical dispositions of the aromatic molecules within the π–π stacks. Subtle changes in these constitutions or co-conformations will qualitatively alter the charge transport behaviour and induce large variations in conductance, thus providing a strong basis for the design of future electromechanical single-supermolecule devices[2]. In a host–guest strategy (FIG. 5d), π-stacked systems can be engineered[204–206] by accommodating different guest molecules that have

undergone self-assembly inside molecular cages. The distinct benefit of this supramolecular arrangement is the ease of changing the through-space charge transport by merely replacing the guest molecules. When identical aromatic guest molecules are used, the complexes exhibit good conductivities with only a moderate loss in conductance on increasing the number of guest molecules[204]. By contrast, by inserting different pairs of guest molecules into the cages, electronic rectification can be realized[205], originating from the particular stacking orders of different guest molecules. The host–guest strategy adds flexible tunability of functions, for example from a resistor to a rectifier, to single-supermolecule electronic devices.

π–π dimers[222] (FIG. 5e, top left) are another easily accessible supramolecular system on which to investigate through-space charge transport. Unlike the covalently defined conformations present in foldamers or the restricted co-conformations in host–guest complexes, π–π dimers are bound only by π–π interactions between adjacent molecules, which are weak and sensitive to their environments. Experimentally, π–π dimers have been investigated[222,226] by accident on account of neglecting the density of molecules on the electrodes, which has resulted in the conductance of these dimers being unwittingly interpreted as coming from single molecules. Rigorous experiments — performed by removing one of the anchoring groups attached to the electrodes at the end of a molecular wire[207] — verified that intermolecular π–π coupling is strong enough to sustain currents. The intermolecular charge transport paths can be confirmed[209] by flicker noise analysis. Notably, on account of their sensitivity to their environments, we emphasize the importance of taking into account the steric hindrance[210], packing behaviour[227], molecular concentrations[228], solvent effects[229] and electrical measuring modes[230] when discussing the single-supermolecule conductances of π–π dimers. All these factors affect charge transport, and the alteration of any one of them may lead to the modulation of the electronic properties.

The conductances of π–π dimers can be manipulated in a more precise way by adjusting the overlapping of the monomeric π-backbones attached to electrodes (FIG. 5e, top left). The coupling of their frontier molecular orbitals allows a quantum interference oscillation[208,227] along the breaking direction of the π–π dimer junction. This manipulation of electrodes that control the conductances[213] also works perfectly at 2D bilayer graphene junctions (FIG. 5e, bottom left), demonstrating pronounced oscillations of conductances with amplitudes that undergo a modulation of over an order of magnitude with respect to the displacement of the electrodes (FIG. 5e, right). Further potential applications related to other 2D materials, such as vertically stacked 2D heterojunctions and twisted bilayer graphenes, will afford opportunities for the development of transistors, photodetectors and superconductors.

In the pursuit of a more comprehensive platform to investigate the quantum transport of molecular 2D materials, an important advance has turned out to be the fabrication of atomically defined 2D electrodes associated with single-molecule junctions. In this case, graphene has been chosen[231] for the construction of 2D nanoscale electrodes based on MCBJ platforms to implement the cross-plane break-junction technique, in which guest molecules are sandwiched between the 2D graphene electrodes so as to form graphene–molecule–graphene van der Waals heterojunctions (FIG. 5f, bottom). The cross-plane charge transport, which takes place by means of phase-coherent tunnelling processes and involves π–π overlap between the graphene electrodes and the guest molecules, is detected as being distinct from conventional in-plane charge transport, providing more information on through-space transport phenomena. Importantly, the sandwiched guest molecules — which include polycyclic aromatic hydrocarbons[232], fullerenes[231] and in the future 2D materials — can be extended to afford an extensive molecular library (FIG. 5f, top), opening up new opportunities for exploiting the structure–property relationship of through-space π-conjugation.

Charge transport in stacked sequences of nucleic acids. DNA represents a large family of naturally occurring π-stacked supermolecules in which the base pairs carrying the genetic information are also bound by multiple hydrogen bonds. Long-distance charge transport through double-helical DNA has received a lot of attention[217,221,233–235] because of its unique properties — including self-assembly, self-replication, self-reparation and inherent programmability — that can even lead to the creation of molecular-scale circuitry[236]. The mechanisms by which electrons propagate[217,237] through DNA, however, are still a matter of some controversy. Coherent tunnelling[238] and incoherent hopping[239] have been advanced as the two leading theories to explain[235] the short-range and long-range transport of electrons in DNA, respectively. In the coherent tunnelling regime, the conductance decreases exponentially with the length of DNA chains[238]. This mechanism holds well for DNA that has short length (1–3 nm) and exhibits strong electronic coupling. In the incoherent hopping regime, however, each base acts as a hopping site, and the overall conductance decreases linearly with the increasing length of the DNA chains. In some particular cases, there is a crossover point between these two regimes[32,240,241], where coherent and incoherent transport coexist (FIG. 5g). The existence of such an intermediate tunnelling–hopping regime relies[242] on the strong coupling of π-electrons between adjacent base pairs, leading to the delocalization of holes spanning several base pairs in DNA. In addition to charge transport, coherent spin transport in DNA has also been observed[243,244], in which the spin selectivity is related to conformational change[245] and oxidative damage[246]. These investigations point to considerable potential for DNA molecules to be applied as efficient spin filters in spintronics.

Various techniques have established[217] that DNA can conduct charges efficiently through its π–π-stacked base pairs, while the charge transport[247,248] reflects a keen sensitivity to the structural integrity associated with π–π stacking interactions. Single-supermolecule electrical measurements, in conjunction with other techniques,

have demonstrated that the sensitivity of charge transport is related to a variety of structural imperfections, which include single-site cleavage[249], single-base mismatch[248] and single-nucleotide polymorphisms[250]. This sensitivity comes[251] primarily from the effects of mutations on changes in the co-conformation of DNA, leading to the disruption of π–π stacking interactions, increasing the tunnelling barrier and decreasing the overall conductance of DNA helices. This unique characteristic can be used to probe the conductance of target RNA sequences directly through hybridization with a single DNA probe[251–253], generating a conductance signature and providing single-nucleotide polymorphism sensitivity (FIG. 5h).

DNA intercalation occurs when aromatic molecules of suitable sizes insert themselves in between the DNA base pairs (FIG. 5i). Intercalation requires the dynamic unwinding of the DNA chains to open up spaces between base pairs, creating openings for the intercalators to centre and bind. Biologically, intercalators often inhibit the repair, transcription and replication of DNA, making them potent mutagens. Electronically, intercalators give rise to perturbations in the structural integrity of DNA and bring about the reorganization of electronic density along the π–π-stacked base-pair sequences. These stereoelectronic changes can induce large variations in the conductance of DNA[220], as well as bestowing upon it specific device properties, such as rectification[31], that natural DNA does not display.

Although considerable progress has been made in the understanding of DNA charge transport mechanisms, as far as real applications in DNA electronics are concerned, the situation remains complicated. An emerging research direction is the investigation[254,255] of the self-assembly of DNA in order to enable the construction of programmable molecular circuits. Early attempts to realize DNA nanocircuits have used the guanine quadruplex[236,256] as the active conducting component. Future efforts could be focused on the integration of DNA electronics with DNA origami[255], as well as exploring the use of programmable DNA circuits for molecular electronics.

MIMs switches and integrated circuits

A couple of decades ago, on account of the ease with which bistability[257] could be introduced synthetically into mechanically interlocked molecules[28], a fruitful marriage[29,258–260] took place between molecular switches[27,261–266] in the form of bistable MIMs and single-molecule electronics[267]. The resulting union expanded the reach of MIMs beyond their all-important contribution to the rise of molecular machines[27,268–278]. This interdisciplinary research has led[279] to the design and construction of a variety of molecular devices and integrated circuits that include, but are not limited to, photo-switches[280,281] and detectors[282], artificial molecular muscles[57,283], molecular mechanical biosensors[284], electrochromic devices[285,286], single-molecule transistors[287,288], random-access memories[289,290] and configurable logic circuits[289,290]. In this section, we limit our discussion to two kinds of bistable MIMs — bistable [2]catenanes[291] and bistable rotaxanes[263,292,293] — as well as some closely related oligorotaxane foldamers[56,57,294]. We focus primarily on introducing the switching mechanism relating to bistable MIMs and their applications in molecular switch tunnel junctions (MSTJs) and integrated circuits. We also explore the possibility of using multiple non-covalent interactions in the development of MIM-based single-molecule devices.

Binary switching mechanism of bistable MIMs. This story begins in 1999 with the use of a [2]rotaxane monolayer in the fabrication[295] of single-molecule-thick electrochemical junctions that were shown[296] to function as electronically configurable molecular-based logic gates. This achievement in device fabrication led to the establishment of a programme of research focusing on a bistable [2]catenane[291] in which one of the component rings was a macrocyclic polyether containing tetrathiafulvalene (TTF) and 1,5-dioxynaphthalene (DNP) units, whereas the other ring was a tetracationic cyclophane (often referred to as the little blue box): cyclobis(paraquat-*p*-phenylene)[297,298] ($CBPQT^{4+}$). UV/Vis absorption and ^{1}H NMR spectroscopies, performed in MeCN/CD_3CN on this bistable [2]catenane, as its tetrakis(hexafluorophosphate) ($4PF_6^-$) salt, revealed[291] a better than 9:1 preference for the co-conformation (translational isomer) where the TTF unit in the polyether macrocycle resides inside the cavity of the $CBPQT^{4+}$ ring. X-ray diffraction analysis, performed on single crystals of the bistable [2]catenane, showed that it crystallizes in the same co-conformation as the major translational isomer present in solution as indicated by ^{1}H NMR spectroscopy. The catenane can be switched both chemically (using $FeClO_4$ as the oxidant and ascorbic acid as the reductant) and electrochemically between its ground-state co-conformation (GSCC), where the TTF unit occupies the cavity of the $CBPQT^{4+}$ ring, and a metastable co-conformation (MSCC), where the DNP unit is located inside its cavity. The next step was to utilize[299,300] the Langmuir–Blodgett technique[301] to introduce the bistable [2]catenane onto a polysilicon electrode in a solid-state device[302,303]. In order to enhance the stability and uniformity of the [2]catenane Langmuir–Blodgett layer, the PF_6^- anions were replaced by dimyristoylphosphatidyl ($DMPA^-$) anions[299,300,302].

It turns out that it is much easier to introduce the amphiphilicity — required for the application of the Langmuir–Blodgett technique[301] to the fabrication of MSTJs-crossbars — into bistable [2]rotaxanes. To take an example, the amphiphilic bistable [2]rotaxane[292,293] illustrated in FIG. 6a comprises a $CBPQT^{4+}$ ring component (dark blue) and a dumbbell component incorporating TTF (green) and DNP (red) units intercepting a polyether chain that is terminated at one end by a large hydrophobic aromatic stopper (black) and at the other end by an equally large hydrophilic stopper (turquoise). Under ambient conditions in MeCN solution, the $CBPQT^{4+}$ ring encircles the TTF unit in preference to the DNP unit by a factor of approximately 9:1. While the translational isomer in which the $CBPQT^{4+}$ ring encircles the TTF unit corresponds to the GSCC, the isomer in which the $CBPQT^{4+}$ ring encircles the DNP unit corresponds to the MSCC. The equilibrium

between these two co-conformations corresponds to a ΔG value of 1.6 kcal mol^{-1}. Switching between the GSCC and MSCC states can be achieved[292,293] electrochemically in MeCN solution. At positive potentials, the TTF unit is oxidized first to the $TTF^{\bullet+}$ radical cation and then to the TTF^{2+} dication. Coulombic repulsion between the $CBPQT^{4+}$ ring and the $TTF^{\bullet+}$ radical cation causes the ring to move and reside on the DNP unit. On reduction, the $TTF^{\bullet+}$ radical cation returns to its neutral state, and an activated process ensues as the $CBPQT^{4+}$ ring makes its way back to the neutral TTF unit. For the bistable [2]rotaxane shown in FIG. 6a, the activation barrier ($\Delta G^{\neq}$, FIG. 6b) is 16 kcal mol^{-1} in MeCN solution[29] (FIG. 6c). It is important to appreciate that the magnitude of this $\Delta G^{\neq}$ value is dependent on the environment[264,265]. The $\Delta G^{\neq}$ value increases (FIG. 6b) to 18 kcal mol^{-1} when the bistable [2]rotaxane is trapped inside a high-viscoscity, solid-state polymer electrolyte gel, or forms a self-assembled monolayer (SAM) on a gold surface[257], or on metal nanoparticles[304,305] and finally to 21 kcal mol^{-1} when it is fabricated as a monolayer inside a MSTJ device[289]. Switching in MSTJs has also been shown[302] to be temperature dependent: below 200 K switching stops altogether, indicating that there is indeed an activation barrier associated with the bistable molecules situated inside MSTJs, and that the switching is a molecular phenomenon.

The presence and switching of these bistable [2]rotaxanes in closely packed monolayers was not only established by experiment[306,307] but also supported by molecular dynamics simulations of the monolayers, both at the air–water interface[308] and on Au(111) surfaces[309,310]. The structural basis for the molecular switching — namely, the two co-conformations of the bistable [2]rotaxanes or [2]catenanes — leads to two different charge transfer rates based on the energy gap hypothesis[289,302,311]. Whatever the dominant or admixture of charge transport models — coherent tunnelling, incoherent tunnelling or thermally activated hopping — two different HOMO energies lead to the high and low conductivities of the MSCC and GSCC, respectively. The HOMO-based energy barrier is lowered (+350 mV) in the metastable (MSCC) state and raised (+700 mV) in the ground (GSCC) state. Thus, HOMO-mediated hole transport in MIMs supports the qualitative conclusion that the conductance across MSCC monolayers is higher than that across GSCC monolayers.

Monolayer junctions based on MIMs. MSTJs were fabricated (FIG. 6f, right) by depositing a Langmuir–Blodgett monolayer of bistable MIMs on Si bottom electrodes in the form of wires whose width was decreased progressively from 100 nm down to less than 20 nm. Polysilicon was chosen for the bottom electrodes (wires) because of its work function (Si is directly below C in the Periodic Table) supporting the marriage with organic molecules and exploiting the fact that Si alleviates the formation of conducting filaments at high voltages[312–314] and is compatible with most semiconductor manufacturing processes. A 2D crossbar architecture was chosen for the simple reason that it is possible to tile molecular switches in a single monolayer using the Langmuir–Blodgett technique. After the spreading of the monolayer, titanium (Ti) electrodes (wires) were introduced at right angles to the Si electrodes (wires) by sputtering hot Ti metal down on top of the monolayer with the aid of a mask. Evidence from reflection absorption infrared spectroscopy[307] for titanium carbide bond formation implies that the annealing process, which is performed at high temperature, relies on the hydrocarbon chains on the $DMPA^{-}$ anions in the case of bistable [2]catenanes, and on the hydrocarbon-based hydrophobic stoppers in the case of bistable [2]rotaxanes, to protect the molecular switches in the monolayer from the fabrication process. Aluminium was deposited on top of the Ti wires as a protecting layer for the molecules and an adhesion layer to the top electrodes.

In these solid-state devices, it transpires that the MSCC correlates with the low-resistance state, which is consistent with the observed shifting in energy of the HOMO in the TTF unit by 210 mV towards the Fermi level when the $CBPQT^{4+}$ ring returns from encircling the TTF unit to encircling the DNP unit in the GSCC. This co-conformational change leads to a higher electrical conductance at low applied bias for the MSCC in the solid-state devices. The hysteretic remnant molecular signature illustrated in FIG. 6d for a single MSTJ-crossbar device, fabricated from a single monolayer of the bistable [2]rotaxane, results from varying write voltage pulses starting from −2 V to +2 V in 40-mV steps and reading the device at −0.2 V. When the write voltage pulses reach +2 V, the switch closes: that is, most of the molecules leave the high-resistance (low-current) GSCC (open state) and centre the low-resistance (high-current) MSCC (closed state). The remnant molecular signature for a particular device can be cycled routinely around 100 times.

While these results were being reported by a group of researchers delocalized between the University of California Los Angeles (UCLA) and the California Institute of Technology (CALTECH), a different set of devices was being fabricated and tested as part of a collaboration at Hewlett-Packard (HP) in Palo Alto[312–314]. The HP group had access to the same range of amphiphilic molecules, including the bistable [2]rotaxane (FIG. 6a), and used them, along with the Langmuir–Blodgett technique[301], to fabricate their devices. The main difference between the two devices rested in the fact that the HP group used platinum instead of polysilicon as the bottom electrode. The HP devices exhibited large amplitude switching (FIG. 6e) that was independent of temperature and showed no dependence on the nature of the molecules in their devices: that is, dumbbells behaved in the same manner as bistable [2]rotaxanes. The HP group postulated that a physical mechanism — not a chemical one — is responsible for the switching they observed at high bias (±3.5 V) compared with the low-bias (±2 V) switching observed in the case of the UCLA/CALTECH devices. A comparison between the two sets of devices is presented in TABLE 1. For a more in-depth discussion of the differences between these two sets of devices, the reader is referred to a dedicated review[29].

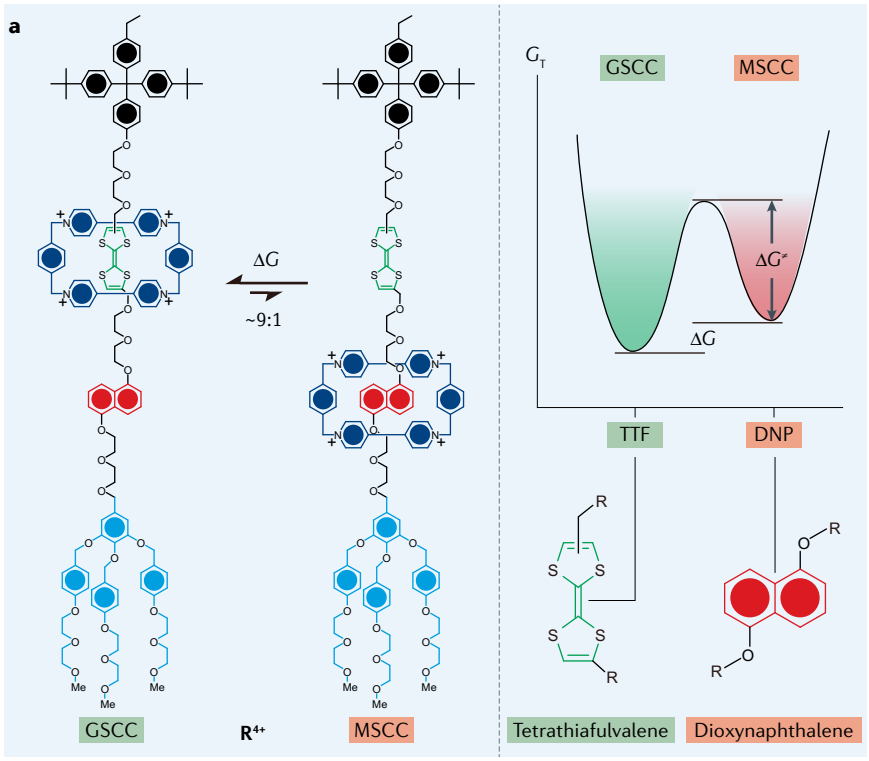
a
ΔG
~9:1
GSCC
R4+
MSCC
Me
G_T
GSCC
MSCC
ΔG‡
ΔG
TTF
DNP
R
S
O
Tetrathiafulvalene
Dioxynaphthalene

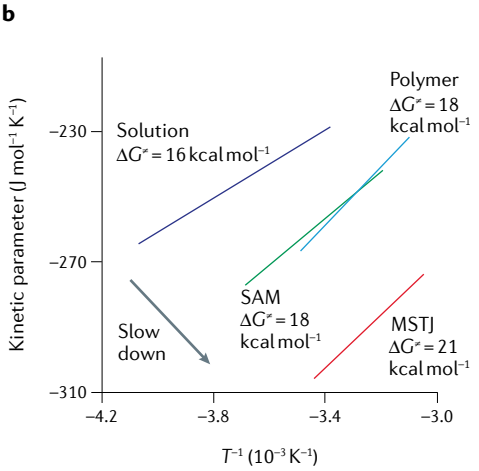
b
Kinetic parameter (J mol⁻¹ K⁻¹)
−230
−270
−310
Solution
ΔG‡ = 16 kcal mol⁻¹
Polymer
ΔG‡ = 18
kcal mol⁻¹
Slow
down
SAM
ΔG‡ = 18
kcal mol⁻¹
MSTJ
ΔG‡ = 21
kcal mol⁻¹
−4.2
−3.8
−3.4
−3.0
T⁻¹ (10⁻³ K⁻¹)

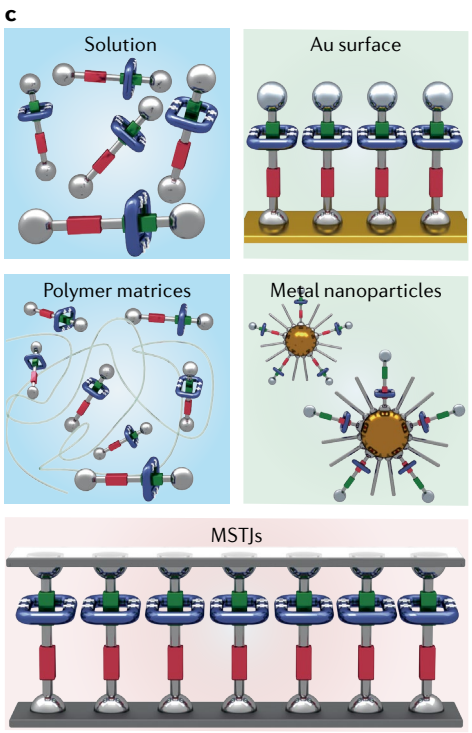
c
Solution
Au surface
Polymer matrices
Metal nanoparticles
MSTJs

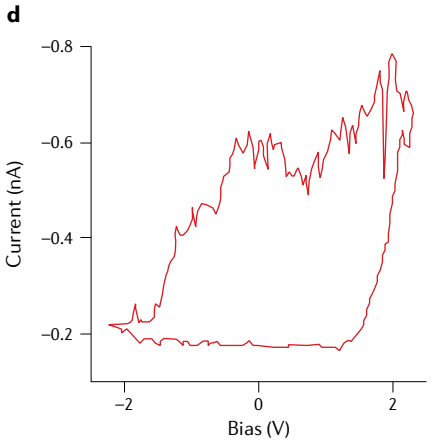
d
Current (nA)
−0.8
−0.6
−0.4
−0.2
−2
0
2
Bias (V)

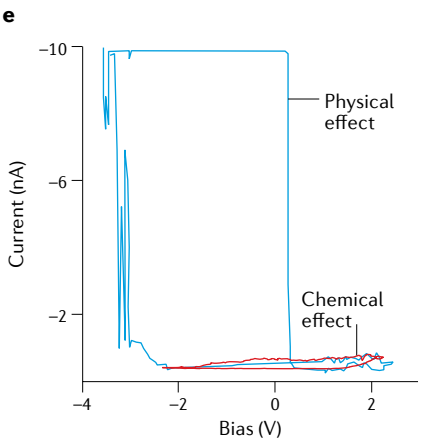
e
Current (nA)
−10
−6
−2
Physical
effect
Chemical
effect
−4
−2
0
2
Bias (V)

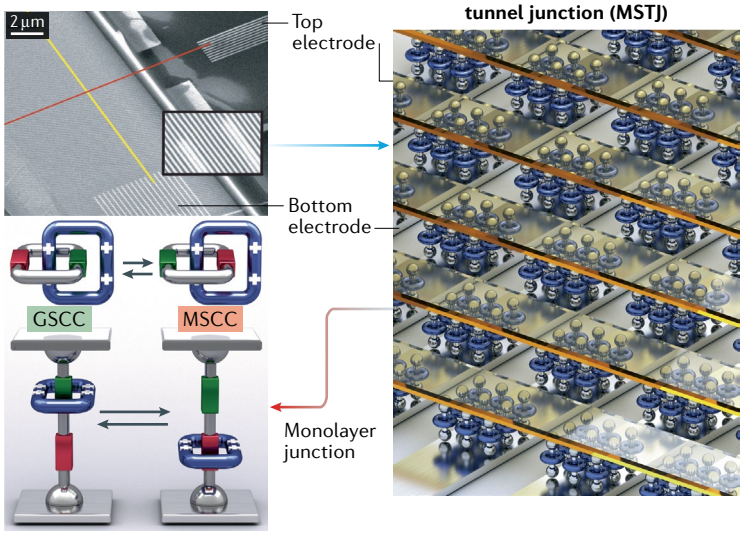
f
2 μm
Top
electrode
Bottom
electrode
GSCC
MSCC
Monolayer
junction
Molecular switch
tunnel junction (MSTJ)

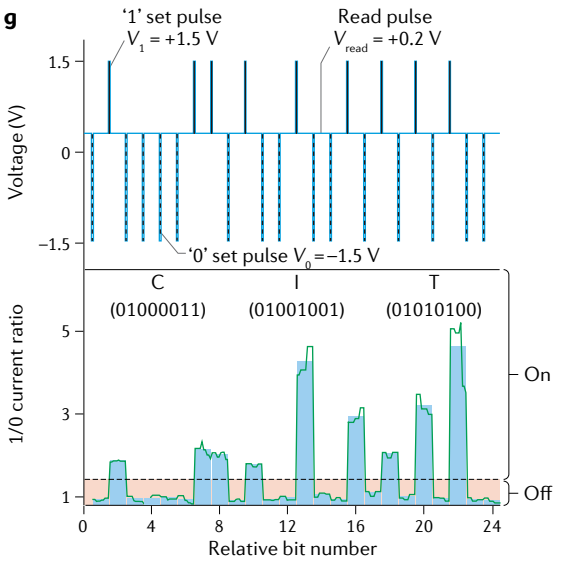
g
'1' set pulse
V_1 = +1.5 V
Read pulse
V_{read} = +0.2 V
Voltage (V)
1.5
0
−1.5
'0' set pulse V_0 = −1.5 V
C
(01000011)
I
(01001001)
T
(01010100)
1/0 current ratio
5
3
1
On
Off
0
4
8
12
16
20
24
Relative bit number

Fig. 6 | **Mechanically interlocked molecule (MIM)-based monolayer junctions and integrated circuits. a** | Structural formulas of the two translational isomers of the amphiphilic bistable [2]rotaxane $\mathbf{R}^{4+}$ in its ground-state co-conformation (GSCC) and metastable co-conformation (MSCC) and the equilibrium between the GSCC and the MSCC in MeCN solution at room temperature (left). Schematic representation (right) of the bistable potential energy surface with potential energy wells corresponding to the GSCC and MSCC (Gibbs free energy: $\Delta G = 1.6\,kcal\,mol^{-1}$, activation barrier: $\Delta G^{\neq} = 16\,kcal\,mol^{-1}$). **b** | Eyring plots and free energy barrier ($\Delta G^{\neq}$) in solution, on a self-assembled monolayer (SAM), in a polymer gel of high viscosity, and in a molecular switch tunnel junction (MSTJ) device. **c** | Schematic illustrations showing the relaxation of bistable rotaxanes from their MSCC states (not illustrated) back to their GSCC states in different physical environments. The bistable rotaxanes can be housed in solution, on SAMs formed on a flat Au surface or on metal nanoparticles, in polymer matrices, and finally in monolayers in MSTJs. **d** | Remnant molecular signature of a MSTJ device incorporating a monolayer of the bistable [2]rotaxane $\mathbf{R}^{4+}$, measured by varying the write voltage from −2 V to +2 V in 40-mV steps, whilst reading the device at −0.2 V. **e** | High-bias switch in a device fabricated by the Hewlett-Packard group (blue trace). Note the abrupt current increase at −3.0 V. The voltage required to open the switch fluctuates from +0.5 V (shown) to +1.5 V. The remnant molecular signature for a device fabricated by the UCLA/CALTECH groups is shown in red. The difference in current flow between the two devices is large. **f** | A MIM-based dynamic random-access memory circuit. Top left, high-resolution scanning electron microscope image of the nanowire crossbar circuit. Bottom left, bistable states of a bistable [2]catenane (top) or a bistable [2]rotaxane (bottom). The GSCC is less conducting than the MSCC. Right, schematic illustration of the integration of MSTJs into a crossbar device. **g** | The switching operation of this memory device. Top, the pulse sequence used to operate the memory device. Bottom, storing ASCII characters to form the acronym 'CIT', for California Institute of Technology, using binary numbers. Panels **a** and **b** are adapted with permission from REF.[265], Wiley. Panels **c** and **e** are adapted with permission from REF.[29], RSC. Panel **d** is adapted with permission from REF.[289], Wiley. Panels **f** (top) and **g** (bottom) are adapted from REF.[290], Springer Nature Limited.

The UCLA/CALTECH devices went on to blaze a pathway towards integrated circuits[289] based on crossbar-containing monolayers of bistable MIMs of increasing complexity, starting with a 4 × 4 crossbar architecture, followed by an 8 × 8 one[289,313]. Scanning electron microscope images show[290] ultra-high-density MSTJ-crossbars formed by the criss-crossing of the top and bottom electrodes (FIG. 6f, top left). In terms of miniaturization, a 400 × 400 crossbar architecture has been produced with wires (electrodes) 16 nm wide[290]. At these dimensions, each cross-point junction (FIG. 6f, right) contains around 200 bistable [2]rotaxane molecules in an area of about 250 square nanometres. All 160,000 junctions, patterned at a density of 10^{11} bits per square centimetre, constitute a 160-kbit molecular memory circuit. This molecular electronic device is operated[289,290] by applying different bias voltages (FIG. 6g), writing with a positive high-voltage pulse, reading at a bias of around 0 V and erasing with a negative high-voltage pulse.

Many technical and engineering challenges — including the junction yields, the robustness of the devices, as well as the stability and uniformity of the electrical performance — remain to be addressed before these crossbar memristors can hope to be accepted as next-generation non-volatile memory candidates. To address these challenges, some non-destructive top-contact fabrication methods, such as metallic nanoparticle contacts[315] or soft-graphene contacts[118], might provide a way forward. These advances provide compelling demonstrations of new concepts for possible applications of molecular memristors in emerging fields, such as bio-inspired computing[316,317], artificial neural networks[318] and security applications[319].

Molecular junctions based on MIMs. At the single-molecule level, MIMs[27,28] represent a special class of molecules that display a wide range of different intramolecular interactions — such as hydrogen bonding[320], donor–acceptor[57] and radical-pairing[66] interactions — within them, despite the fact that they are not supermolecules. Their mechanically interlocked structures are responsible for controlling the positioning and directional motions of their component parts, rendering them prototypical platforms for the investigation of folding dynamics. AFM-based single-molecule spectroscopy has been used[56,57,320,321] to monitor mechanical forces in MIMs with subnanometre resolution (FIG. 7a, left). For example, in a bistable [2]rotaxane[320] (FIG. 7a, right), pulling the ring along the axle of a dumbbell, away from the thermodynamically favoured binding site, has been demonstrated to generate a directional force of 30 picoNewtons. In donor–acceptor oligorotaxanes[57], real-time probing of force fluctuations between folded and unfolded states has helped us in gaining a deeper understanding of the folding dynamics in proteins.

The investigation of the single-molecule electrical properties of MIMs (FIG. 7b, left), however, poses enormous challenges. For molecules that exhibit a non-resonant tunnelling mechanism, the molecular conductance is expected to decrease exponentially with the increase in tunnelling length. In rotaxanes, although the dumbbell is unusually long, conjugation is usually not good and so prevents them from being applied as conducting bridges. We suggest some molecular engineering strategies to tackle this problem. We should consider introducing[322–328] π-conjugated axles into dumbbells (FIG. 7b, right) in order to reach the resonant tunnelling regime. Given this constitutional modification, the conductance of rotaxanes could be improved considerably. It might lead, however, to limited differences in the conductance between the GSCC and the MSCC of bistable [2]rotaxanes during the switching process. Only more experiments will provide answers.

Perhaps oligorotaxane foldamers[48,66] (FIG. 7c, left) — with radical-pairing interactions to regulate the length and conductance — could be used to create marked binary electrical response between bistable states, leading to larger on/off ratios. Introducing radical chemistry could lead to the development[21,329] of conducting wires, following the discovery[330] of radically conducting polymers. Foldamers enable discrimination between the folded (on state) and stretched (off state) conformations (FIG. 7c, right). More importantly, the foldamer strategy allows direct probing of the subtle differences between tunnelling and hopping mechanisms, as well as between through-space and through-bond transport behaviour during molecular actuation. Also, a foldamer strategy (FIG. 7d) — realized[331] in the segregated stacking of π-conjugated donor and acceptor units — could drive the exploration of single-molecule optoelectronic and ferroelectric[332] properties in MIMs. The family of MIMs, with multiple tunable structures and functions, provides an infinite number of possibilities for next-generation molecular and supramolecular electronic devices that have a good chance of finding real applications.

Table 1 | **Comparison between UCLA/CALTECH and HP devices**

	UCLA/CALTECH devices	HP devices
Electrode materials	Bottom: polysilicon or carbon (SWNTs)	Bottom: Pt
	Top: Ti/Al	Top: Ti/Al
Fabrication methods	Electron-beam lithography	Imprinting process
Switching voltages	Low bias: ±2.0 V are stable (at higher voltages high-bias switching is observed	Low bias: ±3.5 V are not stable and move to higher voltages
		High bias: ±7 V are stable, and the devices can be cycled
Switching amplitudes	Between 2 (bistable catenane) and 10 (bistable rotaxanes)	Between 1,000 and 10,000
Temperature dependence	Yes — no switch operates below 200 K, indicating that there is an activation barrier	No — indicating that there is no activation barrier
Memory effect	Volatile. Relaxing from the closed to open states in a period of 10–60 min	Non-volatile
Switching materials	Only bistable catenanes and rotaxanes switch	All molecules — including degenerate catenanes and dumbbell components of rotaxanes — switch
Switching mechanism	Molecular switching — an electromechanical mechanism	Electrode switching — formation of nanofilaments most likely

SWNTs, single-walled carbon nanotubes.

Future perspectives

If supramolecular electronics is to become a productive field of research that leads to new technologies, then physical scientists and electronic engineers must acquire an appreciation of the subtleties of non-covalent interactions in MIMs, and also beyond the molecule in supramolecular assemblies of molecules. By the same token, chemists and materials scientists need to familiarize themselves with how best to design and synthesize molecules and supermolecules for their seamless introduction into electronic circuitry by learning about the art of molecular electronics, which involves break-junction platforms, breaking traces and conductance measurements, to mention only a few of the well-established practices in this niche field.

From a theoretical standpoint, models that can fully explain experimental results in supramolecular systems at a quantitative level are needed urgently. Supramolecular electronics will face many of the same issues that molecular electronics has faced in relation to theory. In particular, it is more difficult to simulate or model supramolecular systems through full ab initio approaches. As the size of supermolecules and MIMs increases, the accuracy of the functionals or models decreases substantially. Often one is left with models that yield results several orders of magnitude displaced from experimental results. Why is it so? Can we do better? The continued development of theoretical models, and combined theory–experiment collaborations aimed at solving these problems, will be even more important for supramolecular systems than they have been for much smaller molecules.

The question of how best to achieve a seamless marriage between functional molecules and electronics in devices, so that molecular signatures predominate over all other interfering effects, is one that requires much more serious thought and experimentation. We close this Review by discussing the future directions worthy of exploration in supramolecular electronics: molecular design, technical developments and the drive towards applications.

There is little doubt that MIMs and complexes (supermolecules), with their well-defined structures and superstructures, will continue to be the cornerstones of single-supermolecule electronics. Over the past three decades, hundreds, if not thousands, of molecules have been likened to molecular wires, but only a handful[8–11,13,15–18,333] of them have been investigated electronically in any detail. We propose that at least four supramolecularly related design strategies be addressed with considerable resolve in the next decades. First, we need to continue to use the traditional design concept of molecular bridges, but extend them to encompass the design, synthesis and evaluation of supramolecular switches, rectifiers, transistors and sensors to be able to install them in a range of electronic devices, arrange for these devices to respond to multiple external stimuli and realize their robust operations. Second, it is high time to introduce MIMs, including molecular knots[334], with their unique capabilities to regulate stereoelectronic properties, into the field of molecular electronics. Investigations carried out in break junctions on these 'new' molecules will increase our fundamental understanding of charge transport, especially in the intermediate regime between coherent and incoherent transport. Third, the potential of non-covalent interactions in MIMs and supermolecules should be exploited to the full, in order to install into molecular kernels new charge transport phenomena, for example the possibility of manipulating quantum interference effects in molecules with multiple conducting channels, of using spin-selective transport of dsDNA in spintronics applications, and of exploring the ferroelectric properties of donor–acceptor stacked oligorotaxanes. Fourth and last, designing, assembling and

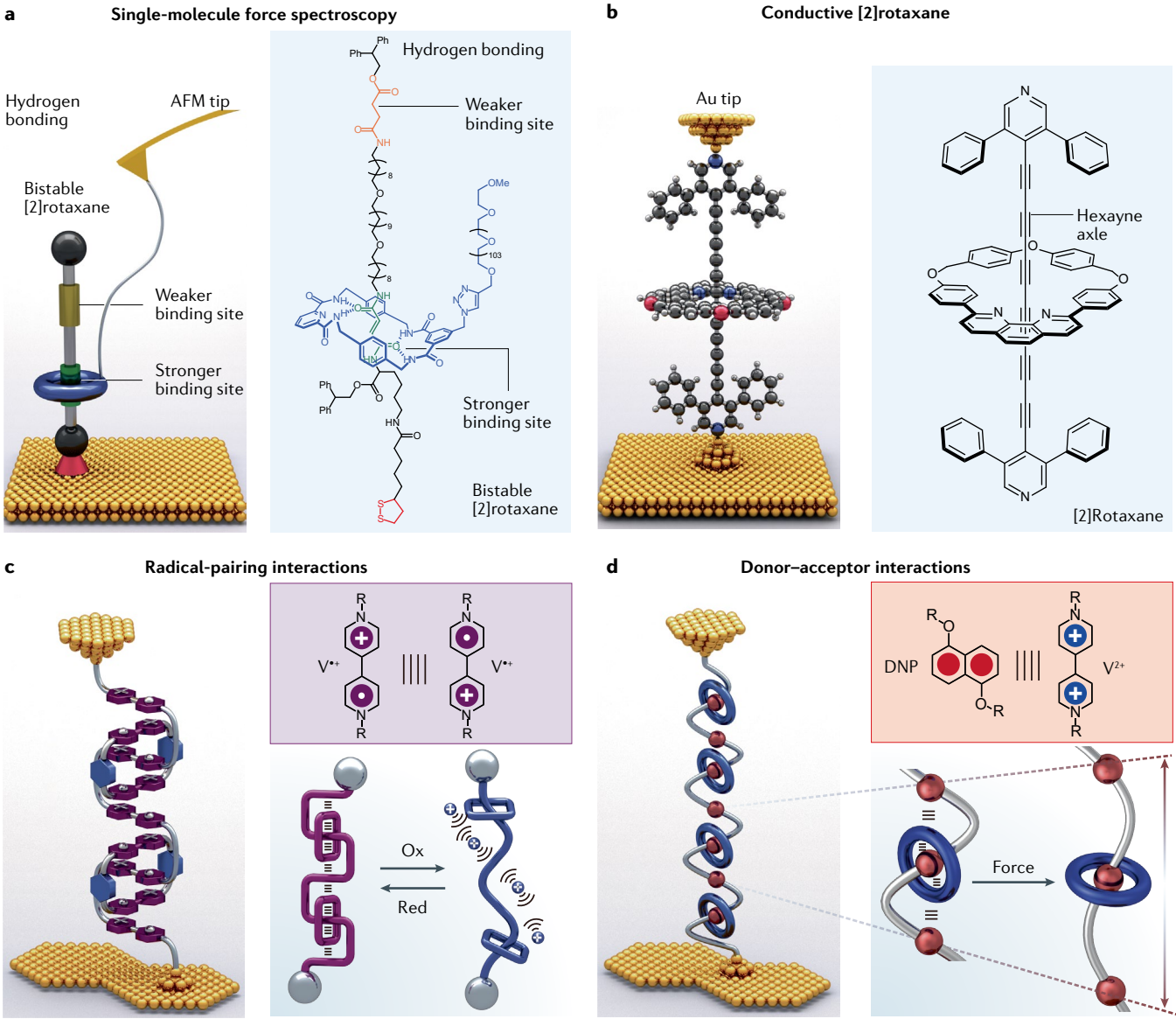

Fig. 7 | **Mechanically interlocked molecule (MIM)-based single-molecule junctions. a** | Single-molecule force spectroscopy performed on a bistable [2]rotaxane. Left, schematic illustration showing the bistable [2]rotaxane grafted onto a Au surface with the polyether chain attached to the atomic force microscope (AFM) tip and stretched by moving the tip away from the surface. Right, structural formula of the bistable [2]rotaxane. The ring can hydrogen-bond to either the fumaramide group (green) or the succinic amide-ester group (orange) as a result of up to four intercomponent hydrogen bonds. **b** | Single-molecule conductance of a [2]rotaxane. Left, schematic illustration showing the scanning tunnelling microscope break junction for measuring the conductance of the [2]rotaxane. Right, structural formula of the [2]rotaxane with its dumbbell incorporating a hexayne axle. **c** | Schematic illustration showing a redox-active oligorotaxane single-molecule junction based on radical-pairing interactions. **d** | Schematic illustration showing a force-triggered oligorotaxane single-molecule junction based on donor–acceptor interactions. V, viologen. Panel **a** is adapted from REF.[320], Springer Nature Limited. Panel **b** is adapted from REF.[323], CC BY 4.0 (https://creativecommons.org/licenses/by/4.0/). Panel **c** is adapted with permission from REF.[66], ACS. Panel **d** is adapted from REF.[57], Springer Nature Limited.

evaluating model supermolecules could help us to gain a better understanding of non-trivial quantum effects in biological systems and their response to physical surroundings within a simplified framework. We advocate increased research activity in the realm of biomolecules, particularly DNA and proteins, which have already been shown to conduct electrons efficiently. Although charge transport in DNA and proteins has been investigated in some detail on single-molecule platforms, the focus has been exclusively on their conductances. The result has been that the fundamental mechanisms relating to biological processes[335] — such as photosynthesis and radical-pairing magnetoreception — remain unclear. It is important that the scientific community focuses on the fundamental research already under way[336,337] in this area during the next decade.

The different non-covalent interactions that coexist in supramolecular assemblies undoubtedly contribute

synergistically to the observed conductances in supermolecules. For example, in DNA, multiple hydrogen bonding exists between two bases, whereas π–π interactions occur within base-pair stacks. Both of these interactions have an impact on charge transport, necessitating their exploration across different technical platforms.

We propose three directions for developing new experimental platforms that go beyond electronic transport considerations. First, we recommend exploiting the advantages of non-covalent interactions to interrogate multiple properties (such as mechanical, optical, thermal and spintronic properties) simultaneously in a supramolecular system, thus advancing our understanding of the superstructure–property relationships governing supramolecular junctions. In addition to this integration strategy involving different techniques, molecular design also needs to be improved and optimized to enable the observation of stable signals across different test platforms for correlation analysis. Second, we recommend using optical trapping techniques to control the movement of single (super)molecules. Optical manipulation of small molecules in nanogaps is challenging but is, nonetheless, worth investigating, with the prospect of there being bonuses for extreme nanophotonics and optoelectronics. Third, to be able to examine the dynamics of charge carriers on extremely short timescales, current measurements need to be synchronized with ultrafast techniques, such as transient absorption, time-resolved photoelectron spectroscopy and terahertz time-domain spectroscopy, to gain more fundamental insight into the dynamics of non-covalent interactions.

Monolayer junctions of MIMs is another field worthy of exploration. MIMs exhibit many of the features of supermolecules because of the presence within them of non-covalent interactions, while maintaining high kinetic and thermodynamic stabilities. We do not need to worry about them dissociating into individual components. Nano-confinement[156] provided by the mechanical bonding in MIMs has led to the stabilization of radical states[338] under ambient conditions. This phenomenon may potentially be incorporated into molecular electronics for the development of next-generation molecular-scale rectifiers, transistors, memory devices and spintronics applications. Also, exploring the memristive properties of monolayer junctions of MIMs may demonstrate their possible application in emerging fields, such as bio-inspired computing, artificial neural networks and security applications. Several technical challenges remain to be addressed before MIM-based crossbar MSTJs can be accepted as a next-generation memristor candidate. These challenges are the relatively low on/off ratios, the slow switching speeds, the robustness of devices, and the uniformity and stability of electrical operations. To address all these issues, some non-destructive fabrication methods and integration strategies need to be developed.

Although slow switching speed can, in principle, be addressed by arranging for many (supra)molecular switches to operate in parallel, rather than in series, and on/off ratios can be raised by an order of magnitude by improved molecular design and repeated experimental evaluation, the establishment of firm chemical platforms that offer open and strong environments in which switchable molecules can be addressed both in terms of writing and reading remotely is needed. The lack of robustness in relation to MIMs is being addressed. Films of switchable main-chain poly[n]rotaxanes, which have already been incorporated into Si-based MSTJ-devices by spin-coating, display hysteretic responses with applied voltages between the GSCC and MSCC conductive states[339]. They offer considerable advantages in synthetic efficiency and ease of fabrication compared with small-molecule rotaxanes[292,293,303]. Aside from incorporating switchable rotaxanes into polymers, it had been suggested back in 2010 in a forward-looking perspective[340] that MIMs can be inserted covalently into the rigid backbones of metal–organic frameworks (MOFs) as integrated components, while preserving their dynamics and not compromising the fidelity of the entire system. The perspective[340], on 'Robust dynamics', prophesies that ultradense, 3D arrays of molecular memories based on switchable MIMs will make their way into state-of-the-art device settings. Evidence that this upbeat message may come to fruition lies in the fact that incorporating long organic struts of up to 2 nm in length — with aromatic-based macrocyclic polyethers as recognition modules fused onto their midriffs — into MOFs has led to their specific binding to methyl viologen[341] in a manner that is not observed in the passive open-reticulated extended structures. Both [2]catenanes[342] and [2]rotaxanes[343,344] have been shown to continue to express the relative movements of their component parts when integrated into the extended structures of MOFs. The most recent advances in this quest for robustness without impairing mechanical motions is the successful application of post-synthetic transformations[345] of bistable MIMs into these highly porous crystalline frameworks. An example[346] is the use of a post-synthetic protocol to introduce a redox-active [2]catenane into a MOF and then demonstrate that its redox-switching is retained, as evidenced by solid-state UV–Vis–NIR reflection spectroscopy and cyclic voltammetry.

During the decades since the publication of the seminal paper by Ari Aviram and Mark Ratner[1] on molecular rectifiers in 1974, molecular electronics has experienced many twists and turns in its development. Ambitious plans are required during the next decade if we are to deepen and extend our understanding of fundamental transport mechanisms and at the same time come up with real applications. DNA and protein sequencing using recognition tunnelling is one of the applications that is close to commercialization. Technical improvements, including the combination of nanopore technology, machine learning and multimode integration, are required in order to improve sequencing performance. The ultimate goal of (supra)molecular electronics — namely, building molecular integrated circuits — is going to require a revolutionary device architecture and an integrated systems approach that must be compatible with the silicon semiconductor industry as we know it today.

Published online 1 April 2021

1. Aviram, A. & Ratner, M. A. Molecular rectifiers. *Chem. Phys. Lett.* **29**, 277–283 (1974).
2. Joachim, C., Gimzewski, J. K. & Aviram, A. Electronics using hybrid-molecular and mono-molecular devices. *Nature* **408**, 541–548 (2000).
3. Flood, A. H., Stoddart, J. F., Steuerman, D. W. & Heath, J. R. Whence molecular electronics? *Science* **306**, 2055–2056 (2004).
4. Joachim, C. & Ratner, M. A. Molecular electronics: some views on transport junctions and beyond. *Proc. Natl Acad. Sci. USA* **102**, 8801–8808 (2005).
5. Ratner, M. A. A brief history of molecular electronics. *Nat. Nanotechnol.* **8**, 378–381 (2013).
6. van der Molen, S. J. et al. Visions for a molecular future. *Nat. Nanotechnol.* **8**, 385–389 (2013).
7. Lambert, C. J. Basic concepts of quantum interference and electron transport in single-molecule electronics. *Chem. Soc. Rev.* **44**, 875–888 (2015).
8. Xiang, D., Wang, X., Jia, C., Lee, T. & Guo, X. Molecular-scale electronics: from concept to function. *Chem. Rev.* **116**, 4318–4440 (2016).
9. Su, T. A., Neupane, M., Steigerwald, M. L., Venkataraman, L. & Nuckolls, C. Chemical principles of single-molecule electronics. *Nat. Rev. Mater.* **1**, 16002 (2016).
10. Xin, N. et al. Concepts in the design and engineering of single-molecule electronic devices. *Nat. Rev. Phys.* **1**, 211–230 (2019).
11. Gehring, P., Thijssen, J. M. & van der Zant, H. S. J. Single-molecule quantum-transport phenomena in break junctions. *Nat. Rev. Phys.* **1**, 381–396 (2019).
12. Feldman, A. K., Steigerwald, M. L., Guo, X. & Nuckolls, C. Molecular electronic devices based on single-walled carbon nanotube electrodes. *Acc. Chem. Res.* **41**, 1731–1741 (2008).
13. Yoshizawa, K. An orbital rule for electron transport in molecules. *Acc. Chem. Res.* **45**, 1612–1621 (2012).
14. Jia, C., Ma, B., Xin, N. & Guo, X. Carbon electrode–molecule junctions: a reliable platform for molecular electronics. *Acc. Chem. Res.* **48**, 2565–2575 (2015).
15. Hybertsen, M. S. & Venkataraman, L. Structure–property relationships in atomic-scale junctions: histograms and beyond. *Acc. Chem. Res.* **49**, 452–460 (2016).
16. Lo, W.-Y., Zhang, N., Cai, Z., Li, L. & Yu, L. Beyond molecular wires: design molecular electronic functions based on dipolar effect. *Acc. Chem. Res.* **49**, 1852–1863 (2016).
17. Su, T. A. et al. Silane and germane molecular electronics. *Acc. Chem. Res.* **50**, 1088–1095 (2017).
18. Liu, J., Huang, X., Wang, F. & Hong, W. Quantum interference effects in charge transport through single-molecule junctions: detection, manipulation, and application. *Acc. Chem. Res.* **52**, 151–160 (2019).
19. Li, Y., Yang, C. & Guo, X. Single-molecule electrical detection: a promising route toward the fundamental limits of chemistry and life science. *Acc. Chem. Res.* **53**, 159–169 (2020).
20. Lehn, J.-M. Supramolecular chemistry — scope and perspectives molecules, supermolecules, and molecular devices (Nobel Lecture). *Angew. Chem. Int. Ed.* **27**, 89–112 (1988).
21. Han, Y. et al. Electric-field-driven dual-functional molecular switches in tunnel junctions. *Nat. Mater.* **19**, 843–848 (2020).
22. Zhou, C. et al. Direct observation of single-molecule hydrogen-bond dynamics with single-bond resolution. *Nat. Commun.* **9**, 807 (2018).
23. Dubecký, M., Mitas, L. & Jurečka, P. Noncovalent interactions by quantum Monte Carlo. *Chem. Rev.* **116**, 5188–5215 (2016).
24. Biedermann, F. & Schneider, H.-J. Experimental binding energies in supramolecular complexes. *Chem. Rev.* **116**, 5216–5300 (2016).
25. Christensen, A. S., Kubař, T., Cui, Q. & Elstner, M. Semiempirical quantum mechanical methods for noncovalent interactions for chemical and biochemical applications. *Chem. Rev.* **116**, 5301–5337 (2016).
26. Rodgers, M. T. & Armentrout, P. B. Cationic noncovalent interactions: energetics and periodic trends. *Chem. Rev.* **116**, 5642–5687 (2016).
27. Stoddart, J. F. Mechanically interlocked molecules (MIMs) — molecular shuttles, switches, and machines (Nobel Lecture). *Angew. Chem. Int. Ed.* **56**, 11094–11125 (2017).
28. Bruns, C. J. & Stoddart, J. F. *The Nature of the Mechanical Bond: From Molecules to Machines* (Wiley, 2016).
29. Coskun, A. et al. High hopes: can molecular electronics realise its potential? *Chem. Soc. Rev.* **41**, 4827–4859 (2012).
30. Aradhya, S. V. & Venkataraman, L. Single-molecule junctions beyond electronic transport. *Nat. Nanotechnol.* **8**, 399–410 (2013).
31. Guo, C. et al. Molecular rectifier composed of DNA with high rectification ratio enabled by intercalation. *Nat. Chem.* **8**, 484–490 (2016).
32. Xiang, L. et al. Intermediate tunnelling–hopping regime in DNA charge transport. *Nat. Chem.* **7**, 221–226 (2015).
33. Chang, S. et al. Tunnelling readout of hydrogen-bonding-based recognition. *Nat. Nanotechnol.* **4**, 297–301 (2009).
34. Zhao, Y. A. et al. Single-molecule spectroscopy of amino acids and peptides by recognition tunnelling. *Nat. Nanotechnol.* **9**, 466–473 (2014).
35. Im, J., Sen, S., Lindsay, S. & Zhang, P. Recognition tunneling of canonical and modified RNA nucleotides for their identification with the aid of machine learning. *ACS Nano* **12**, 7067–7075 (2018).
36. Magoga, M. & Joachim, C. Conductance of molecular wires connected or bonded in parallel. *Phys. Rev. B* **59**, 16011–16021 (1999).
37. Vazquez, H. et al. Probing the conductance superposition law in single-molecule circuits with parallel paths. *Nat. Nanotechnol.* **7**, 663–667 (2012).
38. Chen, H. et al. Giant conductance enhancement of intramolecular circuits through interchannel gating. *Matter* **2**, 378–389 (2020).
39. Zhou, C. et al. Revealing charge- and temperature-dependent movement dynamics and mechanism of individual molecular machines. *Small Methods* **3**, 1900464 (2019).
40. Huang, C., Rudnev, A. V., Hong, W. & Wandlowski, T. Break junction under electrochemical gating: testbed for single-molecule electronics. *Chem. Soc. Rev.* **44**, 889–901 (2015).
41. Tang, J. H. et al. Single-molecule level control of host-guest interactions in metallocycle–C_{60} complexes. *Nat. Commun.* **10**, 4599 (2019).
42. Wang, K. et al. Charge transfer complexation boosts molecular conductance through Fermi level pinning. *Chem. Sci.* **10**, 2396–2403 (2019).
43. Vezzoli, A. et al. Gating of single molecule junction conductance by charge transfer complex formation. *Nanoscale* **7**, 18949–18955 (2015).
44. Tang, Z. et al. Solvent-molecule interaction induced gating of charge transport through single-molecule junctions. *Sci. Bull.* **65**, 944–950 (2020).
45. Makk, P. et al. Correlation analysis of atomic and single-molecule junction conductance. *ACS Nano* **6**, 3411–3423 (2012).
46. Huang, C. C. et al. Single-molecule detection of dihydroazulene photo-thermal reaction using break junction technique. *Nat. Commun.* **8**, 15436 (2017).
47. Zhang, W. et al. Single-molecule conductance of viologen–cucurbit[8]uril host–guest complexes. *ACS Nano* **10**, 5212–5220 (2016).
48. Wang, Y., Frasconi, M. & Stoddart, J. F. Introducing stable radicals into molecular machines. *ACS Cent. Sci.* **3**, 927–935 (2017).
49. Vezzoli, A. et al. Soft versus hard junction formation for α-terthiophene molecular wires and their charge transfer complexes. *J. Chem. Phys.* **146**, 092307 (2017).
50. Nichols, R. J. et al. The experimental determination of the conductance of single molecules. *Phys. Chem. Chem. Phys.* **12**, 2801–2815 (2010).
51. Branton, D. et al. The potential and challenges of nanopore sequencing. *Nat. Biotechnol.* **26**, 1146–1153 (2008).
52. Restrepo-Perez, L., Joo, C. & Dekker, C. Paving the way to single-molecule protein sequencing. *Nat. Nanotechnol.* **13**, 786–796 (2018).
53. Im, J. et al. Electronic single-molecule identification of carbohydrate isomers by recognition tunnelling. *Nat. Commun.* **7**, 13868 (2016).
54. Schönherr, H. et al. Individual supramolecular host–guest interactions studied by dynamic single molecule force spectroscopy. *J. Am. Chem. Soc.* **122**, 4963–4967 (2000).
55. Sluysmans, D. & Stoddart, J. F. The burgeoning of mechanically interlocked molecules in chemistry. *Trends Chem.* **1**, 185–197 (2019).
56. Sluysmans, D., Devaux, F., Bruns, C. J., Stoddart, J. F. & Duwez, A.-S. Dynamic force spectroscopy of synthetic oligorotaxane foldamers. *Proc. Natl Acad. Sci. USA* **115**, 9362–9366 (2018).
57. Sluysmans, D. et al. Synthetic oligorotaxanes exert high forces when folding under mechanical load. *Nat. Nanotechnol.* **13**, 209–213 (2018).
58. Xing, H. et al. Mechanochemistry of an interlocked poly[2]catenane: from single molecule to bulk gel. *CCS Chem.* **1**, 513–523 (2019).
59. Fisher, T. E., Marszalek, P. E. & Fernandez, J. M. Stretching single molecules into novel conformations using the atomic force microscope. *Nat. Struct. Biol.* **7**, 719–724 (2000).
60. Krieg, M. et al. Atomic force microscopy-based mechanobiology. *Nat. Rev. Phys.* **1**, 41–57 (2019).
61. Rubio, G., Agraït, N. & Vieira, S. Atomic-sized metallic contacts: mechanical properties and electronic transport. *Phys. Rev. Lett.* **76**, 2302–2305 (1996).
62. Xu, B., Xiao, X. & Tao, N. J. Measurements of single-molecule electromechanical properties. *J. Am. Chem. Soc.* **125**, 16164–16165 (2003).
63. Aradhya, S. V. et al. Dissecting contact mechanics from quantum interference in single-molecule junctions of stilbene derivatives. *Nano Lett.* **12**, 1643–1647 (2012).
64. Frei, M., Aradhya, S. V., Koentopp, M., Hybertsen, M. S. & Venkataraman, L. Mechanics and chemistry: single molecule bond rupture forces correlate with molecular backbone structure. *Nano Lett.* **11**, 1518–1523 (2011).
65. Aradhya, S. V., Frei, M., Hybertsen, M. S. & Venkataraman, L. Van der Waals interactions at metal/organic interfaces at the single-molecule level. *Nat. Mater.* **11**, 872–876 (2012).
66. Wang, Y. P. et al. Oligorotaxane radicals under orders. *ACS Cent. Sci.* **2**, 89–98 (2016).
67. Quek, S. Y. et al. Mechanically controlled binary conductance switching of a single-molecule junction. *Nat. Nanotechnol.* **4**, 230–234 (2009).
68. Wang, K., Hamill, J., Zhou, J., Guo, C. & Xu, B. Measurement and control of detailed electronic properties in a single molecule break junction. *Faraday Discuss.* **174**, 91–104 (2014).
69. McGraw, J. D., Niguès, A., Chennevière, A. & Siria, A. Contact dependence and velocity crossover in friction between microscopic solid/solid contacts. *Nano Lett.* **17**, 6335–6339 (2017).
70. Comtet, J., Lainé, A., Niguès, A., Bocquet, L. & Siria, A. Atomic rheology of gold nanojunctions. *Nature* **569**, 393–397 (2019).
71. Jia, C. et al. Covalently bonded single-molecule junctions with stable and reversible photoswitched conductivity. *Science* **352**, 1443–1445 (2016).
72. Liu, Z. et al. Revealing the molecular structure of single-molecule junctions in different conductance states by fishing-mode tip-enhanced Raman spectroscopy. *Nat. Commun.* **2**, 305 (2011).
73. Guo, C. et al. Molecular orbital gating surface-enhanced Raman scattering. *ACS Nano* **12**, 11229–11235 (2018).
74. Bi, H. et al. Voltage-driven conformational switching with distinct Raman signature in a single-molecule junction. *J. Am. Chem. Soc.* **140**, 4835–4840 (2018).
75. Bi, H. et al. Electron–phonon coupling in current-driven single-molecule junctions. *J. Am. Chem. Soc.* **142**, 3384–3391 (2020).
76. Jeong, H., Li, H. B., Domulevicz, L. & Hihath, J. An on-chip break junction system for combined single-molecule conductance and Raman spectroscopies. *Adv. Funct. Mater.* **30**, 2000615 (2020).
77. Doppagne, B. et al. Single-molecule tautomerization tracking through space- and time-resolved fluorescence spectroscopy. *Nat. Nanotechnol.* **15**, 207–211 (2020).
78. Qiu, X. H., Nazin, G. V. & Ho, W. Vibrationally resolved fluorescence excited with submolecular precision. *Science* **299**, 542–546 (2003).
79. Marquardt, C. W. et al. Electroluminescence from a single nanotube–molecule–nanotube junction. *Nat. Nanotechnol.* **5**, 863–867 (2010).
80. Reecht, G. et al. Electroluminescence of a polythiophene molecular wire suspended between a metallic surface and the tip of a scanning tunneling microscope. *Phys. Rev. Lett.* **112**, 047403 (2014).
81. Pozzi, E. A. et al. Ultrahigh-vacuum tip-enhanced Raman spectroscopy. *Chem. Rev.* **117**, 4961–4982 (2017).
82. Cram, D. J. & Cram, J. M. Host–guest chemistry. *Science* **183**, 803–809 (1974).
83. Cram, D. J. & Cram, J. M. *Container Molecules and Their Guests* (Royal Society of Chemistry, 1994).
84. Cram, D. J. The design of molecular hosts, guests, and their complexes (Nobel Lecture). *Angew. Chem. Int. Ed.* **27**, 1009–1020 (1988).
85. Kim, J. et al. New cucurbituril homologues: syntheses, isolation, characterization, and X-ray crystal structures of cucurbit[*n*]uril (*n* = 5, 7, and 8). *J. Am. Chem. Soc.* **122**, 540–541 (2000).

86. Chikkaraddy, R. et al. Single-molecule strong coupling at room temperature in plasmonic nanocavities. *Nature* **535**, 127–130 (2016).
87. Baumberg, J. J., Aizpurua, J., Mikkelsen, M. H. & Smith, D. R. Extreme nanophotonics from ultrathin metallic gaps. *Nat. Mater.* **18**, 668–678 (2019).
88. Kim, N. H. et al. Smart SERS hot spots: single molecules can be positioned in a plasmonic nanojunction using host–guest chemistry. *J. Am. Chem. Soc.* **140**, 4705–4711 (2018).
89. Zhang, R. et al. Chemical mapping of a single molecule by plasmon-enhanced Raman scattering. *Nature* **498**, 82–86 (2013).
90. Jiang, S. et al. Distinguishing adjacent molecules on a surface using plasmon-enhanced Raman scattering. *Nat. Nanotechnol.* **10**, 865–869 (2015).
91. Tian, J.-H. et al. Study of molecular junctions with a combined surface-enhanced Raman and mechanically controllable break junction method. *J. Am. Chem. Soc.* **128**, 14748–14749 (2006).
92. Chu, S. The manipulation of neutral particles (Nobel Lecture). *Rev. Mod. Phys.* **70**, 685–706 (1998).
93. Cohen-Tannoudji, C. N. Manipulating atoms with photons (Nobel Lecture). *Rev. Mod. Phys.* **70**, 707–719 (1998).
94. Ketterle, W. When atoms behave as waves: Bose–Einstein condensation and the atom laser (Nobel Lecture). *Rev. Mod. Phys.* **74**, 1131–1151 (2002).
95. Ashkin, A., Dziedzic, J. M., Bjorkholm, J. E. & Chu, S. Observation of a single-beam gradient force optical trap for dielectric particles. *Opt. Lett.* **11**, 288–290 (1986).
96. Chu, S., Bjorkholm, J. E., Ashkin, A. & Cable, A. Experimental observation of optically trapped atoms. *Phys. Rev. Lett.* **57**, 314–317 (1986).
97. Grier, D. G. A revolution in optical manipulation. *Nature* **424**, 810–816 (2003).
98. Dholakia, K. & Čižmár, T. Shaping the future of manipulation. *Nat. Photon.* **5**, 335–342 (2011).
99. Juan, M. L., Righini, M. & Quidant, R. Plasmon nano-optical tweezers. *Nat. Photon.* **5**, 349–356 (2011).
100. Ruggeri, F. & Krishnan, M. Entropic trapping of a singly charged molecule in solution. *Nano Lett.* **18**, 3773–3779 (2018).
101. Maragò, O. M. et al. Femtonewton force sensing with optically trapped nanotubes. *Nano Lett.* **8**, 3211–3216 (2008).
102. Yang, A. H. J. et al. Optical manipulation of nanoparticles and biomolecules in sub-wavelength slot waveguides. *Nature* **457**, 71–75 (2009).
103. Pang, Y. & Gordon, R. Optical trapping of a single protein. *Nano Lett.* **12**, 402–406 (2012).
104. Cohen, A. E. & Moerner, W. E. Suppressing Brownian motion of individual biomolecules in solution. *Proc. Natl Acad. Sci. USA* **103**, 4362–4365 (2006).
105. Zhan, C. et al. Single-molecule plasmonic optical trapping. *Matter* **3**, 1350–1360 (2020).
106. Park, J. et al. Coulomb blockade and the Kondo effect in single-atom transistors. *Nature* **417**, 722–725 (2002).
107. Liang, W. J., Shores, M. P., Bockrath, M., Long, J. R. & Park, H. Kondo resonance in a single-molecule transistor. *Nature* **417**, 725–729 (2002).
108. Koole, M., Thijssen, J. M., Valkenier, H., Hummelen, J. C. & van der Zant, H. S. J. Electric-field control of interfering transport pathways in a single-molecule anthraquinone transistor. *Nano Lett.* **15**, 5569–5573 (2015).
109. Xin, N. et al. Tuning charge transport in aromatic-ring single-molecule junctions via ionic-liquid gating. *Angew. Chem. Int. Ed.* **57**, 14026–14031 (2018).
110. Xu, Q. et al. Single electron transistor with single aromatic ring molecule covalently connected to graphene nanogaps. *Nano Lett.* **17**, 5335–5341 (2017).
111. Wen, H. et al. Complex formation dynamics in a single-molecule electronic device. *Sci. Adv.* **2**, e1601113 (2016).
112. Prins, F. et al. Room-temperature gating of molecular junctions using few-layer graphene nanogap electrodes. *Nano Lett.* **11**, 4607–4611 (2011).
113. Lau, C. S. et al. Redox-dependent Franck–Condon blockade and avalanche transport in a graphene–fullerene single-molecule transistor. *Nano Lett.* **16**, 170–176 (2016).
114. Ullmann, K. et al. Single-molecule junctions with epitaxial graphene nanoelectrodes. *Nano Lett.* **15**, 3512–3518 (2015).
115. Thomas, J. O. et al. Understanding resonant charge transport through weakly coupled single-molecule junctions. *Nat. Commun.* **10**, 4628 (2019).
116. Cao, Y. et al. Building high-throughput molecular junctions using indented graphene point contacts. *Angew. Chem. Int. Ed.* **51**, 12228–12232 (2012).
117. El Abbassi, M. et al. Robust graphene-based molecular devices. *Nat. Nanotechnol.* **14**, 957–961 (2019).
118. Jia, C. et al. Quantum interference mediated vertical molecular tunneling transistors. *Sci. Adv.* **4**, eaat8237 (2018).
119. Famili, M. et al. Self-assembled molecular-electronic films controlled by room temperature quantum interference. *Chem* **5**, 474–484 (2019).
120. Jia, C. et al. Redox control of charge transport in vertical ferrocene molecular tunnel junctions. *Chem* **6**, 1172–1182 (2020).
121. Ma, B., Ren, S., Wang, P., Jia, C. & Guo, X. Precise control of graphene etching by remote hydrogen plasma. *Nano Res.* **12**, 137–142 (2019).
122. Lorke, A. et al. Spectroscopy of nanoscopic semiconductor rings. *Phys. Rev. Lett.* **84**, 2223–2226 (2000).
123. Kleemans, N. A. J. M. et al. Oscillatory persistent currents in self-assembled quantum rings. *Phys. Rev. Lett.* **99**, 146808 (2007).
124. Keyser, U. F. et al. Kondo effect in a few-electron quantum ring. *Phys. Rev. Lett.* **90**, 196601 (2003).
125. Wendler, L., Fomin, V. M., Chaplik, A. V. & Govorov, A. O. Optical properties of two interacting electrons in quantum rings: optical absorption and inelastic light scattering. *Phys. Rev. B* **54**, 4794–4810 (1996).
126. Földi, P., Molnár, B., Benedict, M. G. & Peeters, F. M. Spintronic single-qubit gate based on a quantum ring with spin–orbit interaction. *Phys. Rev. B* **71**, 033309 (2005).
127. Souma, S. & Nikolić, B. K. Spin Hall current driven by quantum interferences in mesoscopic Rashba rings. *Phys. Rev. Lett.* **94**, 106602 (2005).
128. Iyoda, M., Yamakawa, J. & Rahman, M. J. Conjugated macrocycles: concepts and applications. *Angew. Chem. Int. Ed.* **50**, 10522–10553 (2011).
129. Spitler, E. L., Johnson, C. A. & Haley, M. M. Renaissance of annulene chemistry. *Chem. Rev.* **106**, 5344–5386 (2006).
130. Mayor, M. & Didschies, C. A giant conjugated molecular ring. *Angew. Chem. Int. Ed.* **42**, 3176–3179 (2003).
131. Peeks, M. D., Claridge, T. D. W. & Anderson, H. L. Aromatic and antiaromatic ring currents in a molecular nanoring. *Nature* **541**, 200–203 (2017).
132. Rickhaus, M. et al. Global aromaticity at the nanoscale. *Nat. Chem.* **12**, 236–241 (2020).
133. Liu, C. et al. Macrocyclic polyradicaloids with unusual super-ring structure and global aromaticity. *Chem* **4**, 1586–1595 (2018).
134. Ni, Y. et al. [n]Cyclo-para-biphenylmethine polyradicaloids: [n]annulene analogs and unusual valence tautomerization. *Chem* **5**, 108–121 (2019).
135. Ni, Y. et al. 3D global aromaticity in a fully conjugated diradicaloid cage at different oxidation states. *Nat. Chem.* **12**, 242–248 (2020).
136. Gryn'ova, G. & Corminboeuf, C. Topology-driven single-molecule conductance of carbon nanothreads. *J. Phys. Chem. Lett.* **10**, 825–830 (2019).
137. Stuyver, T., Perrin, M., Geerlings, P., De Proft, F. & Alonso, M. Conductance switching in expanded porphyrins through aromaticity and topology changes. *J. Am. Chem. Soc.* **140**, 1313–1326 (2018).
138. Okazawa, K., Tsuji, Y. & Yoshizawa, K. Understanding single-molecule parallel circuits on the basis of frontier orbital theory. *J. Phys. Chem. C.* **124**, 3322–3331 (2020).
139. Ellenbogen, J. C. & Love, J. C. Architectures for molecular electronic computers. I. Logic structures and an adder designed from molecular electronic diodes. *Proc. IEEE* **88**, 386–426 (2000).
140. Joachim, C., Gimzewski, J. K. & Tang, H. Physical principles of the single-C_{60} transistor effect. *Phys. Rev. B* **58**, 16407–16417 (1998).
141. Park, H. et al. Nanomechanical oscillations in a single-C_{60} transistor. *Nature* **407**, 57–60 (2000).
142. Joachim, C., Renaud, N. & Hliwa, M. The different designs of molecule logic gates. *Adv. Mater.* **24**, 312–317 (2012).
143. Aviram, A. Molecules for memory, logic, and amplification. *J. Am. Chem. Soc.* **110**, 5687–5692 (1988).
144. Yoshizawa, K., Tada, T. & Staykov, A. Orbital views of the electron transport in molecular devices. *J. Am. Chem. Soc.* **130**, 9406–9413 (2008).
145. Taniguchi, M. et al. Dependence of single-molecule conductance on molecule junction symmetry. *J. Am. Chem. Soc.* **133**, 11426–11429 (2011).
146. Soni, S. et al. Understanding role of parallel pathways via in situ switching of quantum interference in molecular tunneling junctions. *Angew. Chem. Int. Ed.* **59**, 14308–14312 (2020).
147. Pal, A. N. et al. Nonmagnetic single-molecule spin-filter based on quantum interference. *Nat. Commun.* **10**, 5565 (2019).
148. Li, Z. H. et al. Towards graphyne molecular electronics. *Nat. Commun.* **6**, 6321 (2015).
149. Huang, B. et al. Controlling and observing sharp-valleyed quantum interference effect in single molecular junctions. *J. Am. Chem. Soc.* **140**, 17685–17690 (2018).
150. Li, Y. et al. Gate controlling of quantum interference and direct observation of anti-resonances in single molecule charge transport. *Nat. Mater.* **18**, 357–363 (2019).
151. Bai, J. et al. Anti-resonance features of destructive quantum interference in single-molecule thiophene junctions achieved by electrochemical gating. *Nat. Mater.* **18**, 364–369 (2019).
152. Brooke, R. J. et al. Dual control of molecular conductance through pH and potential in single-molecule devices. *Nano Lett.* **18**, 1317–1322 (2018).
153. Li, S. et al. Characterizing intermolecular interactions in redox-active pyridinium-based molecular junctions. *J. Electroanal. Chem.* **875**, 114070 (2020).
154. Hirose, K. A practical guide for the determination of binding constants. *J. Incl. Phenom. Macrocycl. Chem.* **39**, 193–209 (2001).
155. Wei, P., Yan, X. & Huang, F. Supramolecular polymers constructed by orthogonal self-assembly based on host–guest and metal–ligand interactions. *Chem. Soc. Rev.* **44**, 815–832 (2015).
156. Grommet, A. B., Feller, M. & Klajn, R. Chemical reactivity under nanoconfinement. *Nat. Nanotechnol.* **15**, 256–271 (2020).
157. Tromans, R. A. et al. A biomimetic receptor for glucose. *Nat. Chem.* **11**, 52–56 (2019).
158. Therien, M. J., Selman, M., Gray, H. B., Chang, I. J. & Winkler, J. R. Long-range electron transfer in ruthenium-modified cytochrome *c*: evaluation of porphyrin-ruthenium electronic couplings in the *Candida krusei* and horse heart proteins. *J. Am. Chem. Soc.* **112**, 2420–2422 (1990).
159. Kurlancheek, W. & Cave, R. J. Tunneling through weak interactions: comparison of through-space-, H-bond-, and through-bond-mediated tunneling. *J. Phys. Chem. A* **110**, 14018–14028 (2006).
160. Turro, C., Chang, C. K., Leroi, G. E., Cukier, R. I. & Nocera, D. G. Photoinduced electron transfer mediated by a hydrogen-bonded interface. *J. Am. Chem. Soc.* **114**, 4013–4015 (1992).
161. Sessler, J. L., Sathiosatham, M., Brown, C. T., Rhodes, T. A. & Wiederrecht, G. Hydrogen-bond-mediated photoinduced electron-transfer: novel dimethylaniline–anthracene ensembles formed via Watson–Crick base-pairing. *J. Am. Chem. Soc.* **123**, 3655–3660 (2001).
162. Canzi, G. et al. On the observation of intervalence charge transfer bands in hydrogen-bonded mixed-valence complexes. *J. Am. Chem. Soc.* **136**, 1710–1713 (2014).
163. Porter, T. M., Heim, G. P. & Kubiak, C. P. Stable mixed-valent complexes formed by electron delocalization across hydrogen bonds of pyrimidinone-linked metal clusters. *J. Am. Chem. Soc.* **140**, 12756–12759 (2018).
164. Cheng, T. et al. Efficient electron transfer across hydrogen bond interfaces by proton-coupled and -uncoupled pathways. *Nat. Commun.* **10**, 1531 (2019).
165. Derege, P. J. F., Williams, S. A. & Therien, M. J. Direct evaluation of electronic coupling mediated by hydrogen bonds: implications for biological electron-transfer. *Science* **269**, 1409–1413 (1995).
166. Kladnik, G. et al. Ultrafast charge transfer pathways through a prototype amino-carboxylic molecular junction. *Nano Lett.* **16**, 1955–1959 (2016).
167. Nishino, T., Hayashi, N. & Bui, P. T. Direct measurement of electron transfer through a hydrogen bond between single molecules. *J. Am. Chem. Soc.* **135**, 4592–4595 (2013).
168. Zhao, G.-J. & Han, K.-L. Hydrogen bonding in the electronic excited state. *Acc. Chem. Res.* **45**, 404–413 (2012).
169. Migliore, A., Polizzi, N. F., Therien, M. J. & Beratan, D. N. Biochemistry and theory of proton-coupled electron transfer. *Chem. Rev.* **114**, 3381–3465 (2014).
170. Weinberg, D. R. et al. Proton-coupled electron transfer. *Chem. Rev.* **112**, 4016–4093 (2012).

171. Li, Y. et al. Microscopic mechanism of electron transfer through the hydrogen bonds between carboxylated alkanethiol molecules connected to gold electrodes. *J. Chem. Phys.* **141**, 174702 (2014).
172. Wimmer, M., Palma, J. L., Tarakeshwar, P. & Mujica, V. Single-molecule conductance through hydrogen bonds: the role of resonances. *J. Phys. Chem. Lett.* **7**, 2977–2980 (2016).
173. Wang, L. et al. Molecular conductance through a quadruple-hydrogen-bond-bridged supramolecular junction. *Angew. Chem. Int. Ed.* **55**, 12393–12397 (2016).
174. Wu, C. et al. In situ formation of H-bonding imidazole chains in break-junction experiments. *Nanoscale* **12**, 7914–7920 (2020).
175. Jones, L. O., Mosquera, M. A., Schatz, G. C. & Ratner, M. A. Molecular junctions inspired by nature: electrical conduction through noncovalent nanobelts. *J. Phys. Chem. B* **123**, 8096–8102 (2019).
176. Huang, S. et al. Recognition tunneling measurement of the conductance of DNA bases embedded in self-assembled monolayers. *J. Phys. Chem. C.* **114**, 20443–20448 (2010).
177. Grabowski, S. J. What is the covalency of hydrogen bonding? *Chem. Rev.* **111**, 2597–2625 (2011).
178. Pirrotta, A., Vico, L. D., Solomon, G. C. & Franco, I. Single-molecule force-conductance spectroscopy of hydrogen-bonded complexes. *J. Chem. Phys.* **146**, 092329 (2017).
179. Nibbering, E. T. J. & Elsaesser, T. Ultrafast vibrational dynamics of hydrogen bonds in the condensed phase. *Chem. Rev.* **104**, 1887–1914 (2004).
180. Kumagai, T. et al. Thermally and vibrationally induced tautomerization of single porphycene molecules on a Cu(110) surface. *Phys. Rev. Lett.* **111**, 246101 (2013).
181. Kumagai, T. et al. Controlling intramolecular hydrogen transfer in a porphycene molecule with single atoms or molecules located nearby. *Nat. Chem.* **6**, 41–46 (2014).
182. Ladenthin, J. N. et al. Hot carrier-induced tautomerization within a single porphycene molecule on Cu(111). *ACS Nano* **9**, 7287–7295 (2015).
183. Ladenthin, J. N. et al. Force-induced tautomerization in a single molecule. *Nat. Chem.* **8**, 935–940 (2016).
184. Di Ventra, M. & Taniguchi, M. Decoding DNA, RNA and peptides with quantum tunnelling. *Nat. Nanotechnol.* **11**, 117–126 (2016).
185. Huang, S. et al. Identifying single bases in a DNA oligomer with electron tunnelling. *Nat. Nanotechnol.* **5**, 868–873 (2010).
186. Bergstrom, D. E., Zhang, P. & Zhou, J. Synthesis of 2′-deoxy-β-D-ribofuranosyl imidazole and thiazole *C*-nucleosides. *J. Chem. Soc. Perkin Trans.* **1**, 3029–3034 (1994).
187. Liang, F., Li, S., Lindsay, S. & Zhang, P. Synthesis, physicochemical properties, and hydrogen bonding of 4(5)-substituted 1-H-imidazole-2-carboxamide, a potential universal reader for DNA sequencing by recognition tunneling. *Chem. Eur. J.* **18**, 5998–6007 (2012).
188. Biswas, S. et al. Universal readers based on hydrogen bonding or π–π stacking for identification of DNA nucleotides in electron tunnel junctions. *ACS Nano* **10**, 11304–11316 (2016).
189. Tsutsui, M., Taniguchi, M., Yokota, K. & Kawai, T. Identifying single nucleotides by tunnelling current. *Nat. Nanotechnol.* **5**, 286–290 (2010).
190. Taniguchi, M. Combination of single-molecule electrical measurements and machine learning for the identification of single biomolecules. *ACS Omega* **5**, 959–964 (2020).
191. Ivanov, A. P. et al. DNA tunneling detector embedded in a nanopore. *Nano Lett.* **11**, 279–285 (2011).
192. Fanget, A. et al. Nanopore integrated nanogaps for DNA detection. *Nano Lett.* **14**, 244–249 (2014).
193. Garoli, D., Yamazaki, H., Maccaferri, N. & Wanunu, M. Plasmonic nanopores for single-molecule detection and manipulation: toward sequencing applications. *Nano Lett.* **19**, 7553–7562 (2019).
194. Chen, C. et al. High spatial resolution nanoslit SERS for single-molecule nucleobase sensing. *Nat. Commun.* **9**, 1733 (2018).
195. Li, J., Shen, P., Zhao, Z. & Tang, B. Z. Through-space conjugation: a thriving alternative for optoelectronic materials. *CCS Chem.* **1**, 181–196 (2019).
196. Eley, D. D. & Spivey, D. I. Semiconductivity of organic substances. Part 9. Nucleic acid in the dry state. *Trans. Faraday Soc.* **58**, 411–415 (1962).
197. Giri, G. et al. Tuning charge transport in solution-sheared organic semiconductors using lattice strain. *Nature* **480**, 504–508 (2011).
198. Zhang, H. et al. Photocontrol of charge injection/extraction at electrode/semiconductor interfaces for high-photoresponsivity organic transistors. *J. Mater. Chem. C.* **4**, 5289–5296 (2016).
199. Chen, H. et al. Multistep nucleation and growth mechanisms of organic crystals from amorphous solid states. *Nat. Commun.* **10**, 3872 (2019).
200. Ohta, T. et al. Interlayer interaction and electronic screening in multilayer graphene investigated with angle-resolved photoemission spectroscopy. *Phys. Rev. Lett.* **98**, 206802 (2007).
201. Schneebeli, S. T. et al. Single-molecule conductance through multiple π–π-stacked benzene rings determined with direct electrode-to-benzene ring connections. *J. Am. Chem. Soc.* **133**, 2136–2139 (2011).
202. Batra, A. et al. Quantifying through-space charge transfer dynamics in π-coupled molecular systems. *Nat. Commun.* **3**, 1086 (2012).
203. Stefani, D. et al. Large conductance variations in a mechanosensitive single-molecule junction. *Nano Lett.* **18**, 5981–5988 (2018).
204. Kiguchi, M. et al. Electron transport through single molecules comprising aromatic stacks enclosed in self-assembled cages. *Angew. Chem. Int. Ed.* **50**, 5708–5711 (2011).
205. Fujii, S. et al. Rectifying electron-transport properties through stacks of aromatic molecules inserted into a self-assembled cage. *J. Am. Chem. Soc.* **137**, 5939–5947 (2015).
206. Kiguchi, M. et al. Highly conductive [3×*n*] gold-ion clusters enclosed within self-assembled cages. *Angew. Chem. Int. Ed.* **52**, 6202–6205 (2013).
207. Wu, S. et al. Molecular junctions based on aromatic coupling. *Nat. Nanotechnol.* **3**, 569–574 (2008).
208. Frisenda, R., Janssen, V. A. E. C., Grozema, F. C., van der Zant, H. S. J. & Renaud, N. Mechanically controlled quantum interference in individual π-stacked dimers. *Nat. Chem.* **8**, 1099–1104 (2016).
209. Li, X. et al. Structure-independent conductance of thiophene-based single-stacking junctions. *Angew. Chem. Int. Ed.* **59**, 3280–3286 (2020).
210. Martín, S. et al. Identifying diversity in nanoscale electrical break junctions. *J. Am. Chem. Soc.* **132**, 9157–9164 (2010).
211. Carini, M. et al. High conductance values in π-folded molecular junctions. *Nat. Commun.* **8**, 15195 (2017).
212. Méndez-Ardoy, A. et al. Multi-dimensional charge transport in supramolecular helical foldamer assemblies. *Chem. Sci.* **8**, 7251–7257 (2017).
213. Caneva, S. et al. Mechanically controlled quantum interference in graphene break junctions. *Nat. Nanotechnol.* **13**, 1126–1131 (2018).
214. Valli, A., Amaricci, A., Brosco, V. & Capone, M. Interplay between destructive quantum interference and symmetry-breaking phenomena in graphene quantum junctions. *Phys. Rev. B* **100**, 075118 (2019).
215. Caneva, S. et al. A mechanically tunable quantum dot in a graphene break junction. *Nano Lett.* **20**, 4924–4931 (2020).
216. Chen, H., Zhang, W., Li, M., He, G. & Guo, X. Interface engineering in organic field-effect transistors: principles, applications, and perspectives. *Chem. Rev.* **120**, 2879–2949 (2020).
217. Genereux, J. C. & Barton, J. K. Mechanisms for DNA charge transport. *Chem. Rev.* **110**, 1642–1662 (2010).
218. Tsutsui, M. et al. Electrical detection of single methylcytosines in a DNA oligomer. *J. Am. Chem. Soc.* **133**, 9124–9128 (2011).
219. Harashima, T., Kojima, C., Fujii, S., Kiguchi, M. & Nishino, T. Single-molecule conductance of DNA gated and ungated by DNA-binding molecules. *Chem. Commun.* **53**, 10378–10381 (2017).
220. Wang, X., Gao, L., Liang, B., Li, X. & Guo, X. Revealing the direct effect of individual intercalations on DNA conductance toward single-molecule electrical biodetection. *J. Mater. Chem. B* **3**, 5150–5154 (2015).
221. Slinker, J. D., Muren, N. B., Renfrew, S. E. & Barton, J. K. DNA charge transport over 34 nm. *Nat. Chem.* **3**, 228–233 (2011).
222. Emberly, E. G. & Kirczenow, G. Models of electron transport through organic molecular monolayers self-assembled on nanoscale metallic contacts. *Phys. Rev. B* **64**, 235412 (2001).
223. Scullion, L. et al. Large conductance changes in peptide single molecule junctions controlled by pH. *J. Phys. Chem. C.* **115**, 8361–8368 (2011).
224. Chen, L. et al. Multichannel conductance of folded single-molecule wires aided by through-space conjugation. *Angew. Chem. Int. Ed.* **54**, 4231–4235 (2015).
225. Shen, P. et al. Achieving efficient multichannel conductance in through-space conjugated single-molecule parallel circuits. *Angew. Chem. Int. Ed.* **59**, 4581–4588 (2020).
226. Reed, M. A., Zhou, C., Muller, C. J., Burgin, T. P. & Tour, J. M. Conductance of a molecular junction. *Science* **278**, 252–254 (1997).
227. Solomon, G. C., Vura-Weis, J., Herrmann, C., Wasielewski, M. R. & Ratner, M. A. Understanding coherent transport through π-stacked systems upon spatial dislocation. *J. Phys. Chem. B* **114**, 14735–14744 (2010).
228. González, M. T. et al. Structural versus electrical functionalization of oligo(phenylene ethynylene) diamine molecular junctions. *J. Phys. Chem. C.* **118**, 21655–21662 (2014).
229. González, M. T. et al. Break-junction experiments on acetyl-protected conjugated dithiols under different environmental conditions. *J. Phys. Chem. C.* **115**, 17973–17978 (2011).
230. Zheng, J.-T. et al. Electrochemically assisted mechanically controllable break junction studies on the stacking configurations of oligo(phenylene ethynylene)s molecular junctions. *Electrochim. Acta* **200**, 268–275 (2016).
231. Tan, Z. et al. Atomically defined angstrom-scale all-carbon junctions. *Nat. Commun.* **10**, 1748 (2019).
232. Zhao, S. et al. Cross-plane transport in a single-molecule two-dimensional van der Waals heterojunction. *Sci. Adv.* **6**, eaba6714 (2020).
233. Fink, H.-W. & Schönenberger, C. Electrical conduction through DNA molecules. *Nature* **398**, 407–410 (1999).
234. Porath, D., Bezryadin, A., de Vries, S. & Dekker, C. Direct measurement of electrical transport through DNA molecules. *Nature* **403**, 635–638 (2000).
235. Giese, B., Amaudrut, J., Köhler, A.-K., Spormann, M. & Wessely, S. Direct observation of hole transfer through DNA by hopping between adenine bases and by tunnelling. *Nature* **412**, 318–320 (2001).
236. Sha, R. et al. Charge splitters and charge transport junctions based on guanine quadruplexes. *Nat. Nanotechnol.* **13**, 316–321 (2018).
237. Diederichsen, U. Charge transfer in DNA: a controversy. *Angew. Chem. Int. Ed.* **36**, 2317–2319 (1997).
238. Risser, S. M., Beratan, D. N. & Meade, T. J. Electron transfer in DNA: predictions of exponential growth and decay of coupling with donor-acceptor distance. *J. Am. Chem. Soc.* **115**, 2508–2510 (1993).
239. Berlin, Y. A., Burin, A. L. & Ratner, M. A. Charge hopping in DNA. *J. Am. Chem. Soc.* **123**, 260–268 (2001).
240. Kim, H., Kilgour, M. & Segal, D. Intermediate coherent–incoherent charge transport: DNA as a case study. *J. Phys. Chem. C.* **120**, 23951–23962 (2016).
241. Li, Y., Xiang, L., Palma, J. L., Asai, Y. & Tao, N. Thermoelectric effect and its dependence on molecular length and sequence in single DNA molecules. *Nat. Commun.* **7**, 11294 (2016).
242. Renaud, N., Berlin, Y. A., Lewis, F. D. & Ratner, M. A. Between superexchange and hopping: an intermediate charge-transfer mechanism in poly(A)-poly(T) DNA hairpins. *J. Am. Chem. Soc.* **135**, 3953–3963 (2013).
243. Göhler, B. et al. Spin selectivity in electron transmission through self-assembled monolayers of double-stranded DNA. *Science* **331**, 894–897 (2011).
244. Xie, Z. et al. Spin specific electron conduction through DNA oligomers. *Nano Lett.* **11**, 4652–4655 (2011).
245. Zwang, T. J., Hürlimann, S., Hill, M. G. & Barton, J. K. Helix-dependent spin filtering through the DNA duplex. *J. Am. Chem. Soc.* **138**, 15551–15554 (2016).
246. Mishra, S. et al. Effect of oxidative damage on charge and spin transport in DNA. *J. Am. Chem. Soc.* **141**, 123–126 (2019).
247. Arnold, A. R., Grodick, M. A. & Barton, J. K. DNA charge transport: from chemical principles to the cell. *Cell Chem. Biol.* **23**, 183–197 (2016).
248. Guo, X., Gorodetsky, A. A., Hone, J., Barton, J. K. & Nuckolls, C. Conductivity of a single DNA duplex bridging a carbon nanotube gap. *Nat. Nanotechnol.* **3**, 163–167 (2008).
249. Gao, L. et al. Graphene–DNAzyme junctions: a platform for direct metal ion detection with ultrahigh sensitivity. *Chem. Sci.* **6**, 2469–2473 (2015).
250. Hihath, J., Xu, B. Q., Zhang, P. M. & Tao, N. J. Study of single-nucleotide polymorphisms by means of electrical conductance measurements. *Proc. Natl Acad. Sci. USA* **102**, 16979–16983 (2005).

251. Li, Y. et al. Detection and identification of genetic material via single-molecule conductance. *Nat. Nanotechnol.* **13**, 1167–1173 (2018).
252. Li, Y. et al. Comparing charge transport in oligonucleotides: RNA:DNA hybrids and DNA duplexes. *J. Phys. Chem. Lett.* **7**, 1888–1894 (2016).
253. Veselinovic, J. et al. Two-tiered electrical detection, purification, and identification of nucleic acids in complex media. *Electrochim. Acta* **313**, 116–121 (2019).
254. Seeman, N. C. Nanomaterials based on DNA. *Annu. Rev. Biochem.* **79**, 65–87 (2010).
255. Scalise, D. & Schulman, R. Controlling matter at the molecular scale with DNA circuits. *Annu. Rev. Biomed. Eng.* **21**, 469–493 (2019).
256. Livshits, G. I. et al. Long-range charge transport in single G-quadruplex DNA molecules. *Nat. Nanotechnol.* **9**, 1040–1046 (2014).
257. Tseng, H.-R., Wu, D., Fang, N. X., Zhang, X. & Stoddart, J. F. The metastability of an electrochemically controlled nanoscale machine on gold surfaces. *ChemPhysChem* **5**, 111–116 (2004).
258. Beckman, R. et al. Spiers Memorial Lecture — molecular mechanics and molecular electronics. *Faraday Discuss.* **131**, 9–22 (2006).
259. Dichtel, W. R., Heath, J. R. & Stoddart, J. F. Designing bistable [2]rotaxanes for molecular electronic devices. *Phil. Trans. R. Soc. A* **365**, 1607–1625 (2007).
260. Heath, J. R. Molecular electronics. *Annu. Rev. Mater. Res.* **39**, 1–23 (2009).
261. Bissell, R. A., Córdova, E., Kaifer, A. E. & Stoddart, J. F. A chemically and electrochemically switchable molecular shuttle. *Nature* **369**, 133–137 (1994).
262. Pease, A. R. et al. Switching devices based on interlocked molecules. *Acc. Chem. Res.* **34**, 433–444 (2001).
263. Tseng, H.-R., Vignon, S. A. & Stoddart, J. F. Toward chemically controlled nanoscale molecular machinery. *Angew. Chem. Int. Ed.* **42**, 1491–1495 (2003).
264. Flood, A. H. et al. The role of physical environment on molecular electromechanical switching. *Chem. Eur. J.* **10**, 6558–6564 (2004).
265. Choi, J. W. et al. Ground-state equilibrium thermodynamics and switching kinetics of bistable [2] rotaxanes switched in solution, polymer gels, and molecular electronic devices. *Chem. Eur. J.* **12**, 261–279 (2006).
266. Leigh, D. A. Genesis of the nanomachines: the 2016 Nobel prize in chemistry. *Angew. Chem. Int. Ed.* **55**, 14506–14508 (2016).
267. Cuevas, J. C. & Scheer, E. *Molecular Electronics: An Introduction to Theory and Experiment* (World Scientific, 2010).
268. Balzani, V., Credi, A., Raymo, F. M. & Stoddart, J. F. Artificial molecular machines. *Angew. Chem. Int. Ed.* **39**, 3348–3391 (2000).
269. Flood, A. H. et al. Meccano on the nanoscale — a blueprint for making some of the world's tiniest machines. *Aust. J. Chem.* **57**, 301–322 (2004).
270. Kay, E. R., Leigh, D. A. & Zerbetto, F. Synthetic molecular motors and mechanical machines. *Angew. Chem. Int. Ed.* **46**, 72–191 (2007).
271. Balzani, V., Credi, A. & Venturi, M. *Molecular Devices and Machines: Concepts and Perspectives for the Nanoworld*, 2nd edn. (Wiley-VCH, 2008).
272. Coskun, A., Banaszak, M., Astumian, R. D., Stoddart, J. F. & Grzybowski, B. A. Great expectations: can artificial molecular machines deliver on their promise? *Chem. Soc. Rev.* **41**, 19–30 (2012).
273. Kay, E. R. & Leigh, D. A. Rise of the molecular machines. *Angew. Chem. Int. Ed.* **54**, 10080–10088 (2015).
274. Erbas-Cakmak, S., Leigh, D. A., McTernan, C. T. & Nussbaumer, A. L. Artificial molecular machines. *Chem. Rev.* **115**, 10081–10206 (2015).
275. Abendroth, J. M., Bushuyev, O. S., Weiss, P. S. & Barrett, C. J. Controlling motion at the nanoscale: rise of the molecular machines. *ACS Nano* **9**, 7746–7768 (2015).
276. Cheng, C. & Stoddart, J. F. Wholly synthetic molecular machines. *ChemPhysChem* **17**, 1780–1793 (2016).
277. Pezzato, C., Cheng, C., Stoddart, J. F. & Astumian, R. D. Mastering the non-equilibrium assembly and operation of molecular machines. *Chem. Soc. Rev.* **46**, 5491–5507 (2017).
278. Qiu, Y., Feng, Y., Guo, Q.-H., Astumian, R. D. & Stoddart, J. F. Pumps through the ages. *Chem* **6**, 1952–1977 (2020).
279. Coronado, E., Gaviña, P. & Tatay, S. Catenanes and threaded systems: from solution to surfaces. *Chem. Soc. Rev.* **38**, 1674–1689 (2009).
280. Saha, S. & Stoddart, J. F. Photo-driven molecular devices. *Chem. Soc. Rev.* **36**, 77–92 (2007).
281. Sun, J. et al. An electrochromic tristable molecular switch. *J. Am. Chem. Soc.* **137**, 13484–13487 (2015).
282. Jia, C. et al. Interface-engineered bistable [2] rotaxane–graphene hybrids with logic capabilities. *Adv. Mater.* **25**, 6752–6759 (2013).
283. Liu, Y. et al. Linear artificial molecular muscles. *J. Am. Chem. Soc.* **127**, 9745–9759 (2005).
284. Katz, E., Sheeney-Haj-Ichia, L. & Willner, I. Electrical contacting of glucose oxidase in a redox-active rotaxane configuration. *Angew. Chem. Int. Ed.* **43**, 3292–3300 (2004).
285. Steuerman, D. W. et al. Molecular-mechanical switch-based solid-state electrochromic devices. *Angew. Chem. Int. Ed.* **43**, 6486–6491 (2004).
286. Ikeda, T., Higuchi, M. & Kurth, D. G. From thiophene [2]rotaxane to polythiophene polyrotaxane. *J. Am. Chem. Soc.* **131**, 9158–9159 (2009).
287. Yu, H. et al. The molecule–electrode interface in single-molecule transistors. *Angew. Chem. Int. Ed.* **42**, 5706–5711 (2003).
288. Scott, G. D. et al. Mechanism of enhanced rectification in unimolecular Borromean ring devices. *Phys. Rev. B* **74**, 113404 (2006).
289. Luo, Y. et al. Two-dimensional molecular electronics circuits. *ChemPhysChem* **3**, 519–525 (2002).
290. Green, J. E. et al. A 160-kilobit molecular electronic memory patterned at 10^{11} bits per square centimetre. *Nature* **445**, 414–417 (2007).
291. Asakawa, M. et al. A chemically and electrochemically switchable [2]catenane incorporating a tetrathiafulvalene unit. *Angew. Chem. Int. Ed.* **37**, 333–337 (1998).
292. Jeppesen, J. O. et al. Amphiphilic bistable rotaxanes. *Chem. Eur. J.* **9**, 2982–3007 (2003).
293. Jeppesen, J. O., Nygaard, S., Vignon, Scott, A. & Stoddart, J. F. Honing up a genre of amphiphilic bistable [2]rotaxanes for device settings. *Eur. J. Org. Chem.* **2005**, 196–220 (2005).
294. Zhu, Z. et al. Synthesis and solution-state dynamics of donor–acceptor oligorotaxane foldamers. *Chem. Sci.* **4**, 1470–1483 (2013).
295. Wong, E. W. et al. Fabrication and transport properties of single-molecule-thick electrochemical junctions. *J. Am. Chem. Soc.* **122**, 5831–5840 (2000).
296. Collier, C. P. et al. Electronically configurable molecular-based logic gates. *Science* **285**, 391–394 (1999).
297. Odell, B. et al. Cyclobis(paraquat-*p*-phenylene). A tetracationic multipurpose receptor. *Angew. Chem. Int. Ed.* **27**, 1547–1550 (1988).
298. Ashton, P. R. et al. Isostructural, alternately-charged receptor stacks. The inclusion complexes of hydroquinone and catechol dimethyl ethers with cyclobis(paraquat-*p*-phenylene). *Angew. Chem. Int. Ed.* **27**, 1550–1553 (1988).
299. Brown, C. L. et al. Introduction of [2]catenanes into Langmuir films and Langmuir–Blodgett multilayers. A possible strategy for molecular information storage materials. *Langmuir* **16**, 1924–1930 (2000).
300. Asakawa, M. et al. Current/voltage characteristics of monolayers of redox-switchable [2]catenanes on gold. *Adv. Mater.* **12**, 1099–1102 (2000).
301. Talham, D. R. Conducting and magnetic Langmuir–Blodgett films. *Chem. Rev.* **104**, 5479–5502 (2004).
302. Collier, C. P. et al. A [2]catenane-based solid state electronically reconfigurable switch. *Science* **289**, 1172–1175 (2000).
303. Collier, C. P. et al. Molecular-based electronically switchable tunnel junction devices. *J. Am. Chem. Soc.* **123**, 12632–12641 (2001).
304. Klajn, R. et al. Metal nanoparticles functionalized with molecular and supramolecular switches. *J. Am. Chem. Soc.* **131**, 4233–4235 (2009).
305. Coskun, A. et al. Molecular-mechanical switching at the nanoparticle–solvent interface: practice and theory. *J. Am. Chem. Soc.* **132**, 4310–4320 (2010).
306. Huang, T. J. et al. Mechanical shuttling of linear motor-molecules in condensed phases on solid substrates. *Nano Lett.* **4**, 2065–2071 (2004).
307. DeIonno, E., Tseng, H.-R., Harvey, D. D., Stoddart, J. F. & Heath, J. R. Infrared spectroscopic characterization of [2]rotaxane molecular switch tunnel junction devices. *J. Phys. Chem. B* **110**, 7609–7612 (2006).
308. Jang, S. S. et al. Molecular dynamics simulation of amphiphilic bistable [2]rotaxane Langmuir monolayers at the air/water interface. *J. Am. Chem. Soc.* **127**, 14804–14816 (2005).
309. Jang, S. S. et al. Structures and properties of self-assembled monolayers of bistable [2]rotaxanes on Au (111) surfaces from molecular dynamics simulations validated with experiment. *J. Am. Chem. Soc.* **127**, 1563–1575 (2005).
310. Jang, Y. H., Jang, S. S. & Goddard III, W. A. Molecular dynamics simulation study on a monolayer of half [2]rotaxane self-assembled on Au(111). *J. Am. Chem. Soc.* **127**, 4959–4964 (2005).
311. Flood, A. H., Wong, E. W. & Stoddart, J. F. Models of charge transport and transfer in molecular switch tunnel junctions of bistable catenanes and rotaxanes. *Chem. Phys.* **324**, 280–290 (2006).
312. Stewart, D. R. et al. Molecule-independent electrical switching in Pt/organic monolayer/Ti devices. *Nano Lett.* **4**, 133–136 (2004).
313. Chen, Y. et al. Nanoscale molecular-switch crossbar circuits. *Nanotechnology* **14**, 462–468 (2003).
314. Chen, Y. et al. Nanoscale molecular-switch devices fabricated by imprint lithography. *Appl. Phys. Lett.* **82**, 1610–1612 (2003).
315. Puebla-Hellmann, G., Venkatesan, K., Mayor, M. & Lortscher, E. Metallic nanoparticle contacts for high-yield, ambient-stable molecular-monolayer devices. *Nature* **559**, 232–235 (2018).
316. Yang, J. J., Strukov, D. B. & Stewart, D. R. Memristive devices for computing. *Nat. Nanotechnol.* **8**, 13–24 (2013).
317. Wang, Z. et al. Memristors with diffusive dynamics as synaptic emulators for neuromorphic computing. *Nat. Mater.* **16**, 101–108 (2017).
318. Prezioso, M. et al. Training and operation of an integrated neuromorphic network based on metal-oxide memristors. *Nature* **521**, 61–64 (2015).
319. Nili, H. et al. Hardware-intrinsic security primitives enabled by analogue state and nonlinear conductance variations in integrated memristors. *Nat. Electron.* **1**, 197–202 (2018).
320. Lussis, P. et al. A single synthetic small molecule that generates force against a load. *Nat. Nanotechnol.* **6**, 553–557 (2011).
321. Sluysmans, D. et al. Viologen tweezers probing the force of individual donor–acceptor π-interactions. *J. Am. Chem. Soc.* **142**, 21153–21159 (2020).
322. Kiguchi, M. et al. Single-molecule conductance of π-conjugated rotaxane: new method for measuring stipulated electric conductance of π-conjugated molecular wire using STM break junction. *Small* **8**, 726–730 (2012).
323. Milan, D. C. et al. The single-molecule electrical conductance of a rotaxane–hexayne supramolecular assembly. *Nanoscale* **9**, 355–361 (2017).
324. Bernā, J. et al. A catalytic palladium active-metal template pathway to [2]rotaxanes. *Angew. Chem. Int. Ed.* **46**, 5709–5713 (2007).
325. Weisbach, N., Baranová, Z., Gauthier, S., Reibenspies, J. H. & Gladysz, J. A. A new type of insulated molecular wire: a rotaxane derived from a metal-capped conjugated tetrayne. *Chem. Commun.* **48**, 7562–7564 (2012).
326. Movsisyan, L. D. et al. Polyyne rotaxanes: stabilization by encapsulation. *J. Am. Chem. Soc.* **138**, 1366–1376 (2016).
327. Schrettl, S. et al. Facile synthesis of oligoyne amphiphiles and their rotaxanes. *Chem. Sci.* **6**, 564–574 (2015).
328. Woltering, S. L., Gawel, P., Christensen, K. E., Thompson, A. L. & Anderson, H. L. Photochemical unmasking of polyyne rotaxanes. *J. Am. Chem. Soc.* **142**, 13523–13532 (2020).
329. Chen, H. et al. Single-molecule charge transport through positively charged electrostatic anchors. *J. Am. Chem. Soc.* **143**, 2886–2895 (2021).
330. Joo, Y., Agarkar, V., Sung, S. H., Savoie, B. M. & Boudouris, B. W. A nonconjugated radical polymer glass with high electrical conductivity. *Science* **359**, 1391–1395 (2018).
331. Zhu, Z. et al. Oligomeric pseudorotaxanes adopting infinite-chain lattice superstructures. *Angew. Chem. Int. Ed.* **51**, 7231–7235 (2012).
332. Tayi, A. S. et al. Room-temperature ferroelectricity in supramolecular networks of charge-transfer complexes. *Nature* **488**, 485–489 (2012).
333. Frisenda, R., Stefani, D. & van der Zant, H. S. J. Quantum transport through a single conjugated rigid molecule, a mechanical break junction study. *Acc. Chem. Res.* **51**, 1359–1367 (2018).
334. Stoddart, J. F. Dawning of the age of molecular nanotopology. *Nano Lett.* **20**, 5597–5600 (2020).
335. Lambert, N. et al. Quantum biology. *Nat. Phys.* **9**, 10–18 (2013).
336. Fereiro, J. A. et al. Tunneling explains efficient electron transport via protein junctions. *Proc. Natl Acad. Sci. USA* **115**, E4577–E4583 (2018).

337. Lindsay, S. Ubiquitous electron transport in non-electron transfer proteins. *Life* **10**, 72 (2020).
338. Cai, K. et al. Highly stable organic bisradicals protected by mechanical bonds. *J. Am. Chem. Soc.* **142**, 7190–7197 (2020).
339. Zhang, W. et al. A solid-state switch containing an electrochemically switchable bistable poly[*n*]rotaxane. *J. Mater. Chem.* **21**, 1487–1495 (2011).
340. Deng, H., Olson, M. A., Stoddart, J. F. & Yaghi, O. M. Robust dynamics. *Nat. Chem.* **2**, 439–443 (2010).
341. Li, Q. et al. Docking in metal–organic frameworks. *Science* **325**, 855–859 (2009).
342. Zhao, Y.-L. et al. Rigid-strut-containing crown ethers and [2]catenanes for incorporation into metal–organic frameworks. *Chem. Eur. J.* **15**, 13356–13380 (2009).
343. Vukotic, V. N., Harris, K. J., Zhu, K., Schurko, R. W. & Loeb, S. J. Metal–organic frameworks with dynamic interlocked components. *Nat. Chem.* **4**, 456–460 (2012).
344. Zhu, K., O'Keefe, C. A., Vukotic, V. N., Schurko, R. W. & Loeb, S. J. A molecular shuttle that operates inside a metal–organic framework. *Nat. Chem.* **7**, 514–519 (2015).
345. McGonigal, P. R. et al. Electrochemically addressable trisradical rotaxanes organized within a metal–organic framework. *Proc. Natl Acad. Sci. USA* **112**, 11161–11168 (2015).
346. Chen, Q. et al. A redox-active bistable molecular switch mounted inside a metal–organic framework. *J. Am. Chem. Soc.* **138**, 14242–14245 (2016).

Acknowledgements
The authors thank M. E. Schott for feedback on the manuscript, and N. Xin, Y. Jiao, L. Zhang, K. Cai and D. Shen for their discussion and support in preparing the manuscript. The authors also thank Northwestern University for its continuing financial support.

Author contributions
Both authors contributed to all aspects of the manuscript.

Competing interests
The authors declare no competing interests.

Peer review information
Nature Reviews Materials thanks the anonymous reviewers for their contribution to the peer review of this work.

Publisher's note
Springer Nature remains neutral with regard to jurisdictional claims in published maps and institutional affiliations.

© Springer Nature Limited 2021